Iron-Based Amorphous-Metals: High-Performance Corrosion-Resistant Material (HPCRM) Development

J.C. Farmer, J-S. Choi, C. Saw, J. Haslam, D. Day, P. Hailey, T. Lian, R. Rebak, J. Perepezko, J. Payer, D. Branagan, B. Beardsley, A. D'Amato, L. Aprigliano

January 9, 2008

Disclaimer

This document was prepared as an account of work sponsored by an agency of the United States government. Neither the United States government nor Lawrence Livermore National Security, LLC, nor any of their employees makes any warranty, expressed or implied, or assumes any legal liability or responsibility for the accuracy, completeness, or usefulness of any information, apparatus, product, or process disclosed, or represents that its use would not infringe privately owned rights. Reference herein to any specific commercial product, process, or service by trade name, trademark, manufacturer, or otherwise does not necessarily constitute or imply its endorsement, recommendation, or favoring by the United States government or Lawrence Livermore National Security, LLC. The views and opinions of authors expressed herein do not necessarily state or reflect those of the United States government or Lawrence Livermore National Security, LLC, and shall not be used for advertising or product endorsement purposes.

Iron-Based Amorphous-Metals:
High-Performance Corrosion-Resistant Material (HPCRM) Development

Joseph Farmer[1], Jor-Shan Choi[1], Cheng Saw[1], Jeffrey Haslam[1], Dan Day[1], Phillip Hailey[2], Tiangan Lian[3], Raul Rebak[4], John Perepezko[5], Joe Payer[6], Daniel Branagan[7], Brad Beardsley[8], Andy D'Amato[9] and Lou Aprigliano[10]

[1]Lawrence Livermore National Laboratory, Livermore CA; [2]Johnson Controls, Livermore CA; [3]Electric Power Research Institute, Palo Alto CA; [4]General Electric Corporate Research Center, Schenectady NY; [5]University of Wisconsin, Madison WI; [6]Case Western Reserve University, Cleveland OH; [7]The NanoSteel Company, Idaho Falls ID; [8]Caterpillar Incorporated, Peoria IL; [9]Plasma Technology Incorporated, Torrance CA; [10]Strategic Analysis, Arlington VA

Keywords: High-Performance Corrosion-Resistant Materials, HPCRM, Structural Amorphous Metals, SAM, Iron-Based Amorphous-Metal Coatings, Thermal Spray, Applications

Abstract

An overview of the High-Performance Corrosion-Resistant Materials (HPCRM) Program, which was co-sponsored by the Defense Advanced Research Projects Agency (DARPA) Defense Sciences Office (DSO) and the United States Department of Energy (DOE) Office of Civilian and Radioactive Waste Management (OCRWM), is discussed. Programmatic investigations have included a broad range of topics: alloy design and composition; materials synthesis; thermal stability; corrosion resistance; environmental cracking; mechanical properties; damage tolerance; radiation effects; and important potential applications.

Amorphous alloys identified as SAM2X5 ($Fe_{49.7}Cr_{17.7}Mn_{1.9}Mo_{7.4}W_{1.6}B_{15.2}C_{3.8}Si_{2.4}$) and SAM1651 ($Fe_{48}Mo_{14}Cr_{15}Y_2C_{15}B_6$) have been produced as melt-spun ribbons, drop-cast ingots and thermal-spray coatings. Chromium (Cr), molybdenum (Mo) and tungsten (W) additions provided corrosion resistance, while boron (B) enabled glass formation. Earlier electrochemical studies of melt-spun ribbons and ingots of these amorphous alloys demonstrated outstanding passive film stability. More recently thermal-spray coatings of these amorphous alloys have been made and subjected to long-term salt-fog and immersion tests. Good corrosion resistance has been observed during salt-fog testing. Corrosion rates were measured in situ with linear polarization, while simultaneously monitoring the open-circuit corrosion potentials. Reasonably good performance was observed. The sensitivity of these measurements to electrolyte composition and temperature was determined.

The high boron content of this particular amorphous metal makes this amorphous alloy an effective neutron absorber, and suitable for criticality control applications. In general, the corrosion resistance of such iron-based amorphous metals is maintained at operating temperatures up to the glass transition temperature. These materials are much harder than conventional stainless steel and nickel-based materials, and are proving to have excellent wear properties, sufficient to warrant their use in earth excavation, drilling and tunnel boring applications. Large areas have been successfully coated with these materials, with thicknesses of approximately one centimeter. The observed corrosion resistance may enable applications of importance in industries such as: oil and gas production, refining, nuclear power generation, shipping, and others.

Introduction

The outstanding corrosion that may be possible with amorphous metals was recognized several years ago [1-3]. Compositions of several iron-based amorphous metals were published, including several with very good corrosion resistance. Examples included: thermally sprayed coatings of Fe-10Cr-10-Mo-(C,B), bulk Fe-Cr-Mo-C-B, and Fe-Cr-Mo-C-B-P [4-6]. The corrosion resistance of an iron-based amorphous alloy with yttrium (Y), $Fe_{48}Mo_{14}Cr_{15}Y_2C_{15}B_6$ was also been established [7-9]. Yttrium was added to this alloy to lower the critical cooling rate. Several nickel-based amorphous metals have been developed that exhibit exceptional corrosion performance in acids, but have not been included in this study, which is restricted to Fe-based materials. Very good thermal spray coatings of nickel-based crystalline coatings were deposited with thermal spray, but appear to have less corrosion resistance than nickel-based amorphous metals [10].

As pointed out in the literature, an estimate of the relative pitting resistance of alloys can be made using the pitting resistance equivalence number (PREN), which is calculated using the elemental composition of the alloy [11-16]. PREN values for the Fe-based amorphous metals of interest here, and the crystalline reference materials, which include Type 316L stainless steel and Ni-based Alloy C-22, have been calculated using the following equations. Equation 1 has been used for estimating the PREN for nickel-based alloys, and accounts for the beneficial effects of Cr, Mo, W and N on corrosion resistance [13].

$$PREN = [\%Cr] + 3.3 \times [\%Mo + \%W] + 30 \times [\%N] \qquad (1)$$

However, this equation was used to predict comparable corrosion resistance for Alloys C-276 and Alloy C-22, while Alloy C-22 was known to be more corrosion resistant. An equation that has been used to make reasonable predictions of the relative corrosion resistance of austenitic stainless steels and nickel-based alloys such as Alloy C-22 is [14].

$$PREN = [\%Cr] + 3.3 \times ([\%Mo] + 0.5 \times [\%W]) + k \times [\%N] \qquad (2)$$

The factor k is an adjustable parameter used to account for the beneficial effects of nitrogen. Reasonable values of the factor k range from 12.8 to 30, with 16 being accepted as a reasonable value [15]. Estimates used to guide this alloy development were based on the assumption that the value of k is 16. PREN values calculated with Equation 2 indicated that the resistance of the SAM2X5 and SAM1651 amorphous metal formulations should be more resistant to localized corrosion than Type 316L stainless steel or nickel-based Alloy C-22. As in the case of crystalline Fe-based and Ni-based alloys, it was found experimentally that the addition of Cr, Mo, and W substantially increased the corrosion resistance of these amorphous alloys. Additional passive film stability may have been observed, which cannot be attributed to composition alone, and may be attributable to the glassy structure. Additional work is required to further understand the relative roles of composition and crystalline structure in high-performance amorphous metal coatings, such as the ones discussed here. An obvious deficiency associated with the use of a parameter based on chemical composition alone to assess the relative corrosion resistance of both crystalline and amorphous alloys is that microstructure effects on passive film breakdown are ignored. The lack of crystalline structure is believed to be a key attribute of corrosion resistant amorphous metals.

The High-Performance Corrosion-Resistant Materials (HPCRM) Program has developed a family of iron-based amorphous metals with very good corrosion resistance that can be applied as a protective thermal spray coating. Contributions of various research institutions, univesities and corporations are illustrated with Figure 1. Several promising formulations within this alloy family were formed by addition chromium (Cr), molybdenum (Mo), and tungsten (W) for enhanced corrosion resistance, and boron (B) to enable glass formation and neutron absorption. Compositions explored during this study include: SAM35 ($Fe_{54.5}Mn_2Cr_{15}Mo_2W_{1.5}B_{16}C_4Si_5$); SAM40 ($Fe_{52.3}Mn_2Cr_{19}Mo_{2.5}W_{1.7}B_{16}C_4Si_{2.5}$); SAM2X5 ($Fe_{49.7}Cr_{17.7}Mn_{1.9}Mo_{7.4}W_{1.6}B_{15.2}C_{3.8}Si_{2.4}$); SAM6 ($Fe_{43}Cr_{16}Mo_{16}B_5C_{10}P_{10}$); SAM7 or SAM1651 ($Fe_{48}Mo_{14}Cr_{15}Y_2C_{15}B_6$); and SAM10 ($Fe_{57.3}Cr_{21.4}Mo_{2.6}W_{1.8}B_{16.9}$). The parent alloys for preparing this series of amorphous alloys is known as SAM40 ($Fe_{52.3}Cr_{19}Mn_2Mo_{2.5}W_{1.7}B_{16}C_4Si_{2.5}$) and was originally developed by Branagan [17-18]. Examples of amorphous alloy compositions are given in Table 1.

Compositions with high concentration of boron and good corrosion resistance, such SAM2X5 and SAM1651, may have beneficial for applications such as the long-term storage of spent nuclear fuel with enhanced criticality safety [19-22]. In regard to such high temperature applications, it has been shown that the corrosion resistance of such iron-based amorphous metals is maintained at operating temperatures up to the glass transition temperature [19-20]. The upper operating temperature for such materials is believed to be about 570°C ($T_g \approx 579°C$). Above the crystallization temperature ($T_x \approx 628°C$), deleterious crystalline phases formed, and the corrosion resistance was lost.

Experimental Studies

Melt Spun Ribbons

Maximum cooling rates of one million Kelvin per second (10^6 K/s) have been achieved with melt spinning, which is an ideal process for producing amorphous metals over a very broad range of compositions. This process was used to synthesize completely amorphous, Fe-based, corrosion-resistant alloys with near theoretical density, and thereby enabled the effects of coating morphology on corrosion resistance to be separated from the effects of elemental composition. The melt-spun ribbon (MSR) samples produced with this equipment were several meters long, several millimeters wide and approximately 150 microns thick.

Thermal Spray Coatings

The coatings discussed here were made with the high-velocity oxy-fuel (HVOF) process, which involves a combustion flame, and is characterized by gas and particle velocities that are three to four times the speed of sound (mach 3 to 4). This process is ideal for depositing metal and cermet coatings, which have typical bond strengths of 5,000 to 10,000 pounds per square inch (5-10 ksi), porosities of less than one percent (< 1%) and extreme hardness. The cooling rate that can be achieved in a typical thermal spray process such as HVOF are on the order of ten thousand Kelvin per second (10^4 K/s), and are high enough to enable many alloy compositions to be deposited above their respective critical cooling rate, thereby maintaining the vitreous state. However, the range of amorphous metal compositions that can be processed with HVOF is more restricted than those that can be produced with melt spinning, due to the differences in achievable cooling rates. Both kerosene and hydrogen have been investigated as fuels in the HVOF process used to deposit SAM2X5.

Prototypical Thermal Spray Coatings

The coatings discussed here were made with the high-velocity oxy-fuel (HVOF) process, which involves a combustion flame, and is characterized by gas and particle velocities that are three to four times the speed of sound (mach 3 to 4). This process is ideal for depositing metal and cermet coatings, which have typical bond strengths of 5,000 to 10,000 pounds per square inch (5-10 ksi), porosities of less than one percent (< 1%) and extreme hardness. The cooling rate that can be achieved in a typical thermal spray process such as HVOF are on the order of ten thousand Kelvin per second (10^4 K/s), and are high enough to enable many alloy compositions to be deposited above their respective critical cooling rate, thereby maintaining the vitreous state. However, the range of amorphous metal compositions that can be processed with HVOF is more restricted than those that can be produced with melt spinning, due to the differences in achievable cooling rates. Both kerosene and hydrogen have been investigated as fuels in the HVOF process used to deposit SAM2X5 and SAM1651. Type 316L stainless-steel cylinders were coated with SAM2X5, and served as half-scale models of containers for the storage of spent nuclear fuel. SAM2X5-coated cylinders and plates were subjected to eight (8) full cycles in the GM salt fog test (Figure 1). The results of salt-fog testing will be discussed in a subsequent section of this paper. A prototypical half-scale, half-length basket assembly, sized to fit inside the half-scale container, is also shown (Figure 2).
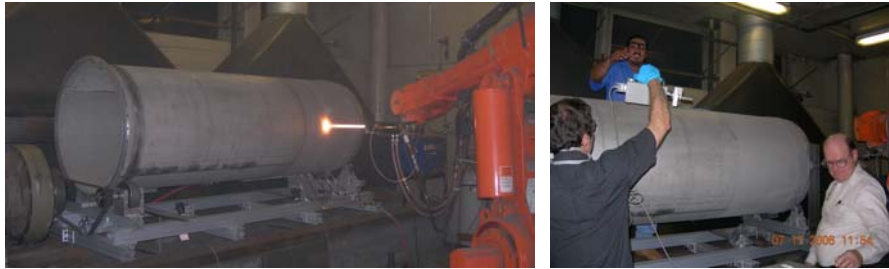

Figure 1 – High-velocity oxy-fuel process at Caterpillar used to coat half-scale containers with SAM1651 amorphous metal. The torch is shown in the left frame, and quality assurance checks of the coating thickness and roughness are shown in the right frame [Beardsley et al. 2006].
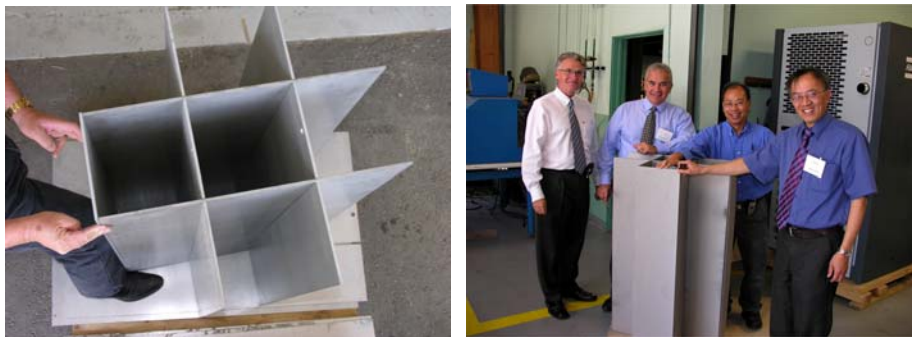

Figure 2 – Prototypical half-scale half-length basket assembly, sized to fit inside the half-scale containers: (a) after fabrication by water-jet cutting; and (b) after coating with SAM2X5 [Choi et al. 2006].

X-Ray Diffraction

The basic theory for X-ray diffraction (XRD) of amorphous materials is well developed and has been published in the literature [23-24]. In an amorphous material, there are broad diffraction peaks. During this study, XRD was done with CuK_α X-rays, a graphite analyzing crystal, and a Philips vertical goniometer, using the Bragg-Bretano method. The X-ray optics were self-focusing, and the distance between the X-ray focal point to the sample position was equal to the distance between the sample position and the receiving slit for the reflection mode. Thus, the intensity and resolution was optimized. Parallel vertical slits were added to improve the scattering signal. Step scanning was performed from 20 to 90° (2θ) with a step size of 0.02° at 4 to 10 seconds per point, depending on the amount of sample. The samples were loaded into low-quartz holder since the expected intensity was very low, thus requiring that the background scattering be minimized. X-ray diffraction (XRD) of Fe-based amorphous-metal melt-spun ribbon (MSR) samples is given as Figure 3 [C. K. Saw et al. 2006]. These data show amorphous structure, with the absence of crystalline phases known to be detrimental to corrosion performance.
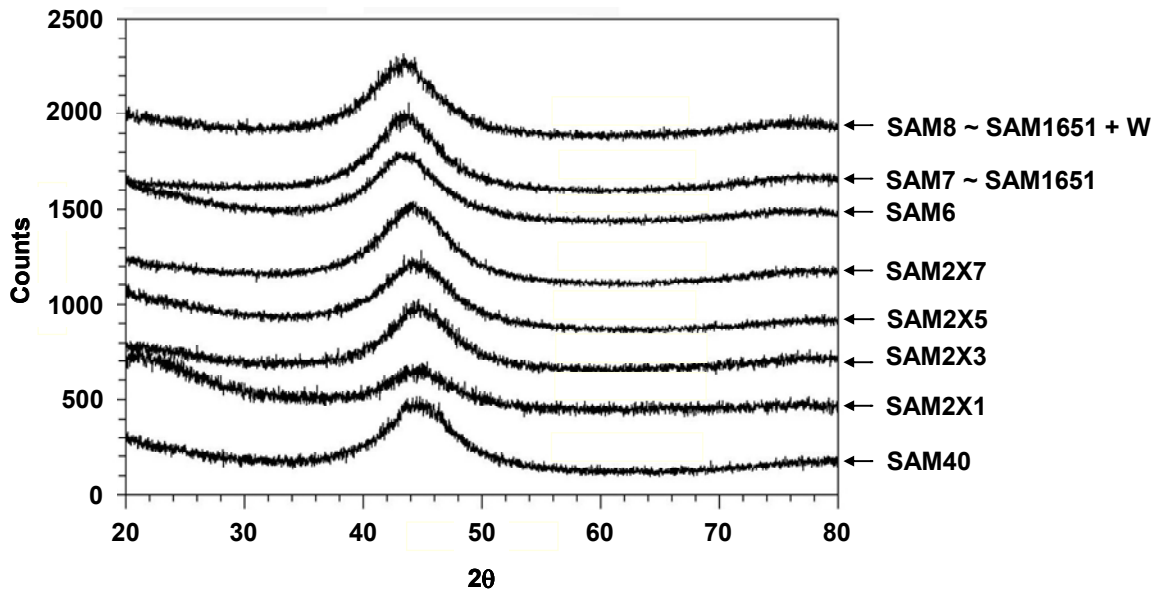

Figure 3 – XRD of Fe-based amorphous-metal MSR samples shows amorphous structure, with the absence of crystalline phases known to be detrimental to corrosion performance [C. K. Saw et al.2006]

A wide variety of standardized coating samples were made for corrosion testing (Figure 4). Samples of the powders used are in the bottles at the top. Crevice samples with a bolt hole in the center are shown on the left. Alloy C-22 rods coated with SAM2X5 and SAM1651 used to monitor open-circuit corrosion potentials and corrosion rates, as determined with linear polarization, are shown on the right. Weight loss samples used for long-term immersion testing are shown in the front center. Ultra-thick (~ 0.75 cm) coatings are also shown, slightly to the right of center.

X-ray diffraction (XRD) measurements of SAM2X5 powder (Lot # 06-015) and thermal-spray coatings made by depositing that powder on Alloy C-22 and Type 316L stainless steel substrates were made and are shown Figure 5. In regard to the thermal-spray coatings, the broad halo observed at 2θ ~ 44° indicated that the coating was predominately amorphous, and the small sharp peaks are attributed to the presence of minor crystalline phases. These phases are believed to include Cr_2B, WC, $M_{23}C_6$ and bcc ferrite, which are known to have a detrimental effect on corrosion performance. These potentially deleterious precipitates deplete the amorphous matrix of those alloying elements, such as chromium, responsible for enhanced passivity. Coatings with less residual crystalline phase have been observed.

Figure 4 – Samples of amorphous-metal HVOF coatings used for long-term corrosion testing.
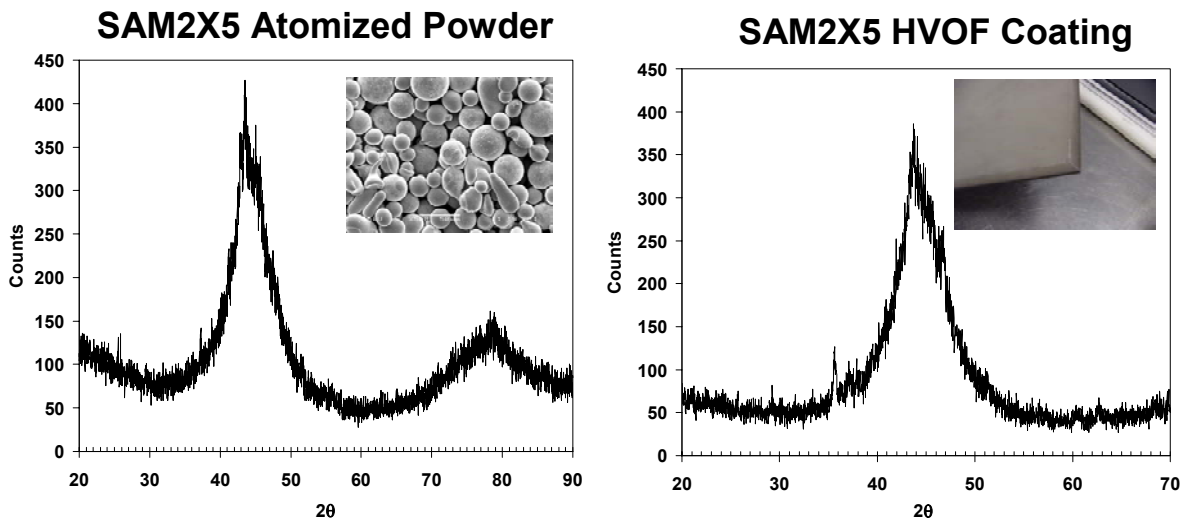

Figure 5 – X-ray diffraction data for amorphous SAM2X5 powder (left) and coating produced from that powder (right). Corrosion performance depends upon the amorphous nature of the material, and is compromised by the presence of Cr_2B, WC, $M_{23}C_6$ and bcc ferrite [C. K. Saw et al. 2006].

Thermal Analysis

The thermal properties of these Fe-based amorphous metals have also been determined by Perepezko et al. [19]. Thermal analysis of these Fe-based amorphous metals, with differential scanning calorimetry (DSC) or differential thermal analysis (DTA), allowed determination of important thermal properties such as the glass transition temperature (T_g), crystallization temperature (T_x), and the melting point (T_m). Results from the thermal analysis of amorphous samples provided initial assessment of the glass forming ability of these materials through conventional metrics, such as the reduced glass transition temperature ($T_{rg} = T_g/T_L$).

The yttrium-containing SAM1651 formulation has a glass transition temperature of ~584°C, a crystallization temperature of ~653°C, a melting point of ~1121°C, and a reduced glass transition temperature of ~0.55. The critical cooling rate of SAM1651 has been determined to be $\leq$ 80 K per second, which is significantly less than other corrosion-resistant iron-based amorphous metals such as SAM2X5. Clearly, the yttrium additions in SAM1651 enhance glass-forming ability of these materials [19].

As an example, the thermal properties of for the SAM2X-series alloys are summarized in Table 1. SAM2X5 ($Fe_{49.7}Cr_{17.7}Mn_{1.9}Mo_{7.4}W_{1.6}B_{15.2}C_{3.8}Si_{2.4}$) had a glass transition temperature of ~579°C, a crystallization temperature of ~628°C, a melting point of ~1133°C, and a reduced glass transition temperature of ~0.57. SAM2X7 had a glass transition temperature of ~573°C, a crystallization temperature of ~630°C, a melting point of ~1137°C, and a reduced glass transition temperature of 0.57. As the Mo additions to SAM40 were increased from 1 to 7 atomic percent, the crystallization temperature increased from ~620 to ~630°C, and the melting point increased from 1110 to 1137°C. Other trends with composition were less obvious. The critical cooling rates for these alloys have been determined to be ~610 Kelvin per second [20].

Table 1 – Thermal properties of SAM40 parent alloy, SAM2X-series of alloys, and SAM1651 [Perepezko et al. 2005]

Alloy	T_g (°C)	T_x (°C)	T_m (°C)	T_L (°C)	T_{rg}
SAM40	568-574	623	1110	1338	0.53
SAM2X1	575	620	1124	1190-1210	0.57
SAM2X3	578	626	1131	1190-1210	0.57
SAM2X5	579	628	1133	1190-1210	0.57
SAM2X7	573	630	1137	1190-1210	0.57
SAM1651	584	653	1121	1290	0.55

Cyclic Polarization

The resistance to localized corrosion is quantified through measurement of the open-circuit corrosion potential (E_{corr}), the breakdown or critical potential ($E_{critical}$), and the repassivation potential (E_{rp}). Spontaneous breakdown of the passive film and localized corrosion require that the open-circuit corrosion potential exceed the critical potential:

$$E_{corr} \geq E_{critical} \qquad\qquad (2)$$

The greater the difference between the open-circuit corrosion potential and the critical potential (ΔE), the more resistant a material is to modes of localized corrosion such a pitting and crevice corrosion. In integrated corrosion models, general corrosion is invoked when E_{corr} is less than $E_{critical}$ ($E_{corr} < E_{critical}$), and localized corrosion is invoked when E_{corr} exceeds $E_{critical}$. Measured values of the repassivation potential (E_{rp}) are sometimes used as conservative estimates of the critical potential ($E_{critical}$) [25].

Different bases exist for determining the critical potential from electrochemical measurements. The breakdown or critical potential has been defined as the potential where the passive current density increases to a level between 1 to 10 μA/cm^2 (10^{-6} to 10^{-5} A/cm^2) while increasing potential in the positive (anodic) directing during cyclic polarization or potential-step testing. The repassivation potential has been defined as the potential where the current density drops to a level indicative of passivity, which has been *assumed* to be between 0.1 to 1.0 μA/cm^2 (10^{-6} to 10^{-7} A/cm^2), while decreasing potential from the maximum level reached during cyclic polarization or potential-step testing [25-26]. An alternate definition of the repassivation potential is: the potential during cyclic polarization where the forward and reverse scans intersect, a point where the measured current density during the reverse scan drops to a level *known* to be indicative of passivity.

Cyclic polarization (CP) measurements was based on a procedure similar to ASTM (American Society for Testing and Materials) G-5 and other similar standards, with slight modification [27]. The ASTM G-5 standard calls for a 1N H_2SO_4 electrolyte, whereas synthetic bicarbonate, sulfate-chloride, chloride-nitrate, and chloride-nitrate solutions, with sodium, potassium and calcium cations, as well as natural seawater were used for this investigation. The natural seawater used in these tests was obtained directly from Half Moon Bay along the northern coast of California. Furthermore, the ASTM G-5 standard calls for the use of de-aerated solutions, whereas aerated and de-aerated solutions were used here. In regard to current densities believed to be indicative of passivity, all data was interpreted in a manner consistent with the published literature.

Temperature-controlled borosilicate glass (Pyrex) electrochemical cells were used for cyclic polarization and other similar electrochemical measurements. This cell had three electrodes, a working electrode (test specimen), a reference electrode, and a counter electrode. A standard silver silver-chloride electrode, filled with near-saturation potassium chloride solution, was used as the reference, and communicated with the test solution via a Luggin probe placed in close proximity to the working electrode, which minimized Ohmic losses. The electrochemical cell was equipped with a water-cooled junction to maintain reference electrode at ambient temperature, which thereby maintained integrity of the potential measurement, and a water-cooled condenser, which prevented the loss of volatile species from the electrolyte.

Cyclic polarization (CP) data for three Fe-based amorphous-metal MSR samples in 5M CaCl$_2$ at 105°C, including SAM27, SAM2X5, and SAM40, are given in Figure 6. The SAM2X5 has enhanced Mo concentration. MSR samples with higher Mo content have superior corrosion performance. A comparison of differences between the observed repassivation potential and corrosion potential for MSR samples of Fe-based amorphous metal in 5M CaCl$_2$ at 105°C is given in Figure 7. Data for other alloys and non-MSR amorphous metal samples are provided in these figures for comparison.

CP data for two wrought Alloy C-22 samples and a SAM2X7 MSR in natural seawater at 30°C is shown in Figure 8. In general, the measured current densities for the SAM2X series of iron-based amorphous-metal melt-spun ribbons were less than those measured for wrought samples of Alloy C-22, indicating better passivity of the amorphous metals. The anodic oxidation peaks for SAM2X7 (see previous figure) and Alloy C-22 are believed to be due to the oxidation of molybdenum.

CP data for two wrought Alloy C-22 samples, and an as-sprayed HVOF coating of SAM2X5, which was deposited on a Type 316L stainless steel substrate, in natural seawater at 90°C is shown in Figure 9. In general, the measured current density for the iron-based amorphous-metal thermal-spray coating in heated seawater was less than those measured for wrought samples of Alloy C-22, indicating better passivity of HVOF SAM2X5 coating in this particular environment. The distinct anodic oxidation peaks for Alloy C-22, and the faint peak for the SAM2X5 thermal spray coating, are all believed to be due to the oxidation of molybdenum.
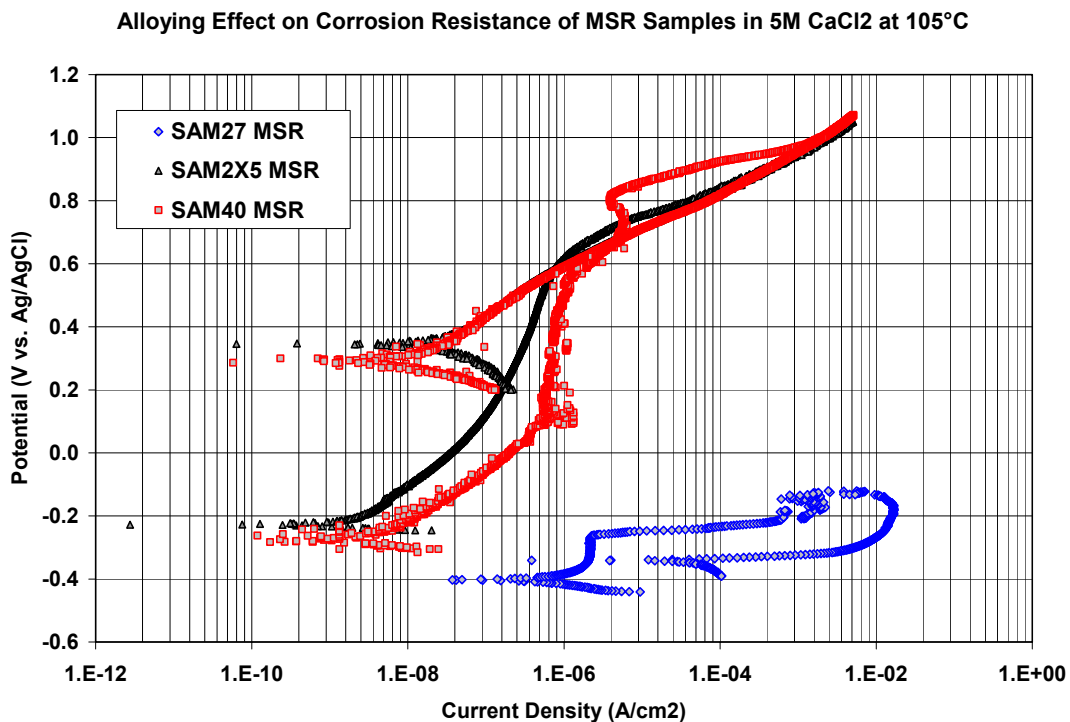

Alloying Effect on Corrosion Resistance of MSR Samples in 5M CaCl2 at 105°C

Figure 6 – CP of three Fe-based amorphous-metal MSR samples in 5M CaCl$_2$ at 105°C: SAM27, SAM2X5, and SAM40. The SAM2X5 has enhanced Mo concentration. MSR samples with higher Mo content have superior corrosion performance. [Farmer et al. 2005]
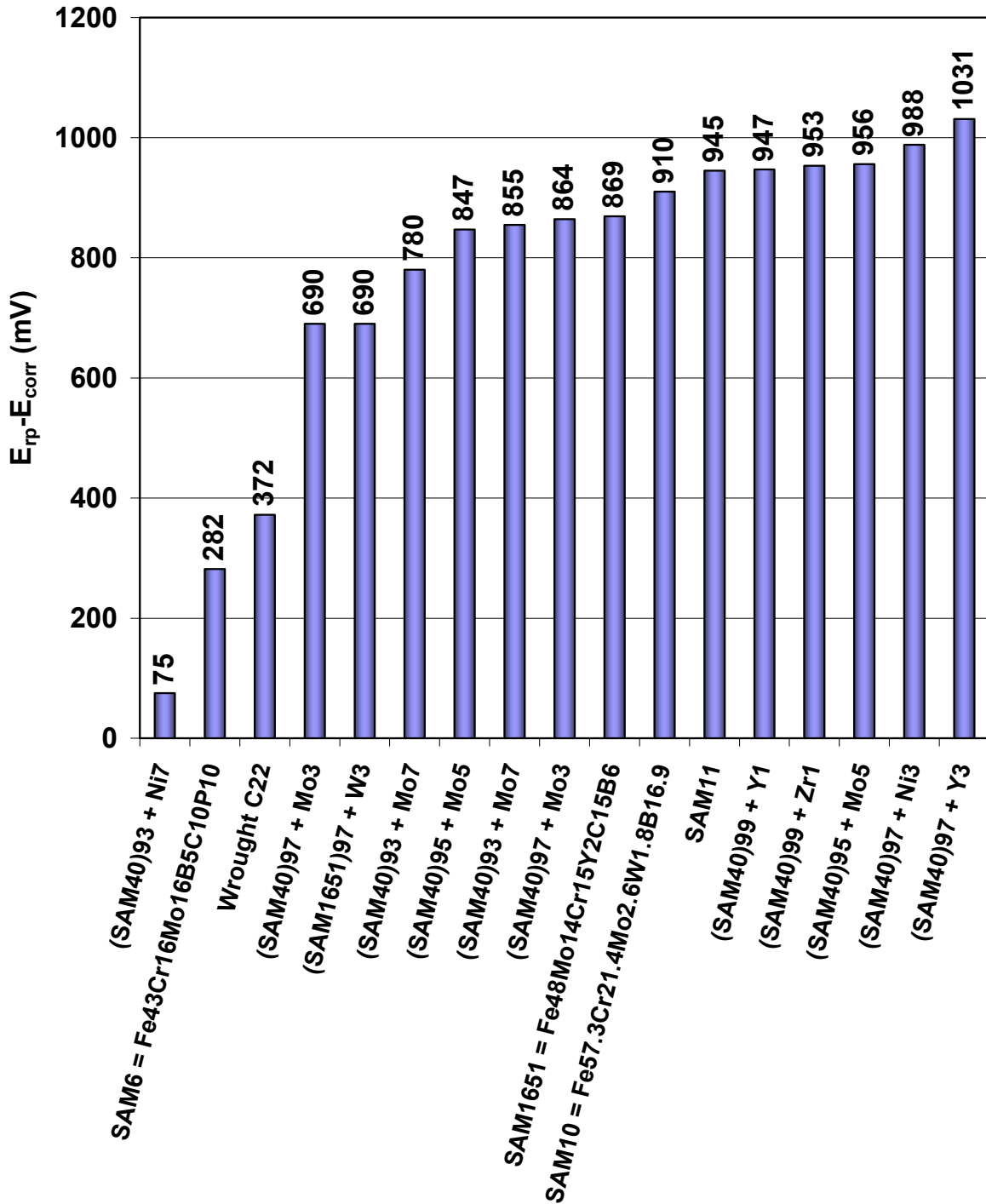
Figure 7 – Comparison of differences between the observed repassivation potential and corrosion potential for MSR samples of Fe-based amorphous metal in 5M CaCl₂ at 105°C, deduced from cyclic polarization data. Other alloys and non-MSR amorphous metal samples are provided for comparison [Farmer et al. 2004].
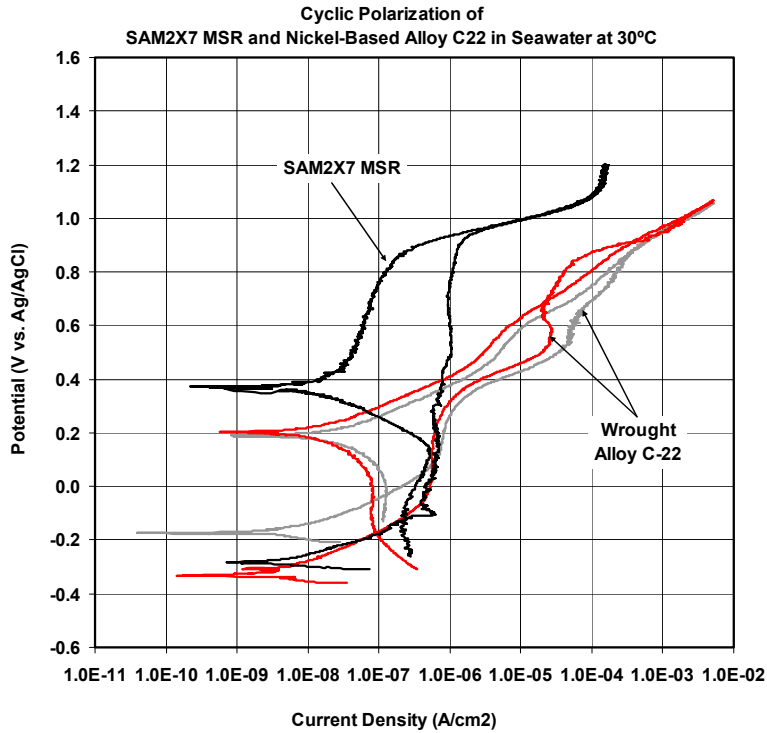
**Cyclic Polarization of
SAM2X7 MSR and Nickel-Based Alloy C22 in Seawater at 30ºC**

Figure 8 – This figure shows potential-current data for two wrought Alloy C-22 samples, and a SAM2X7 MSR in natural seawater at 30°C [Farmer et al. 2005].

**Cyclic Polarization of As-Sprayed
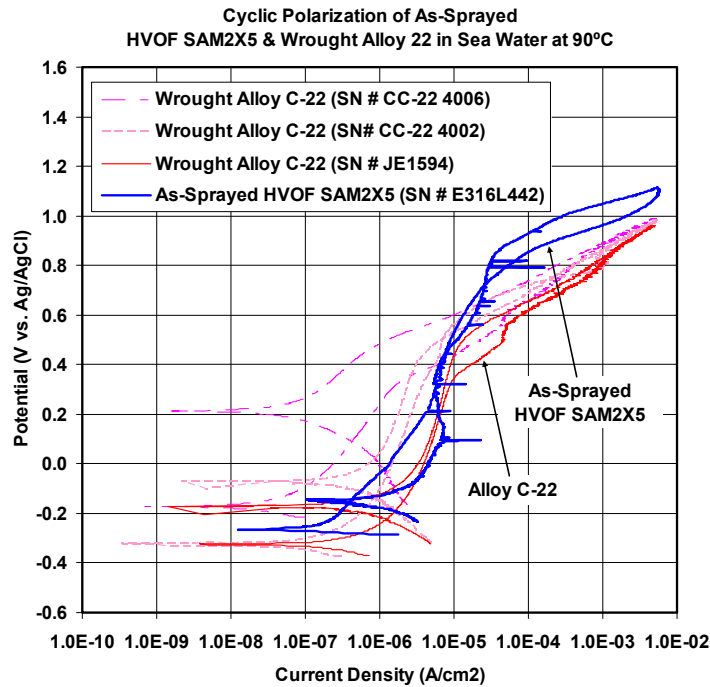HVOF SAM2X5 & Wrought Alloy 22 in Sea Water at 90ºC**

Figure 9 – This figure shows potential-current data for two wrought Alloy C-22 samples, and an as-sprayed HVOF coating of SAM2X5, which was deposited on a Type 316L stainless steel substrate, in natural seawater at 90°C [Farmer et al. 2006].

11

Potential Step Testing

Potential-step testing has been performed on wrought Alloy C-22 (reference material); fully dense and completely amorphous melt spun ribbons of SAM2X5; optimized HVOF coatings produced with −53/+30 micron powders of SAM2X5; and optimized HVOF coatings produced with −30/+15 micron powders of SAM2X5 [28]. All were tested in natural seawater heated to 90°C. To eliminate the need for surface roughness corrections in the conversion of measured current and electrode area to current density, the SAM2X5 and SAM1651 coatings were polished to a 600-grit finish prior to testing. The curves represent the asymptotic current density reached after 24 hours at the corresponding potential (each data point represents a 24 hour test). The constant potential was applied after 1 hour at the open circuit corrosion potential (OCP). It has been found that coatings produced with SAM2X5 powders below a critical size are fully dense and are completely amorphous [28]. The coatings produced with finer powders are therefore expected to have lower porosity and less residual crystalline phases present than those produced with larger particles. These data enable a clear and unambiguous determination of the threshold potentials for passive film breakdown in a non-creviced condition. First, it is clear that the passive film on wrought Alloy C-22 commences breakdown at a potential of approximately 200 mV relative to a standard Ag/AgCl reference electrode (approximately 600 mV above the open circuit corrosion potential), and has the least corrosion resistance of any sample evaluated during this test. Passive film breakdown on the SAM2X5 melt-spun ribbon did not occur until a potential in excess of 1200 mV verses Ag/AgCl (1400 mV above OCP) was applied. Furthermore, the observed passive current density observed with this sample was extremely low. Both HVOF coatings of SAM2X5 (large and small powder sizes) also exhibited outstanding passive film stability, superior to that of the reference material. The passive film on the coating produced with −30/+15 micron powder remained intact until application of 1000 mV verses Ag/AgCl (1200 mV above OCP), with a current density well within the passive range of several microamps per square centimeter. Similar observations were made with the coating produced with −53/+30 micron powders. Any differences in morphology did not have significant impact on corrosion resistance.

Figures 10 and 11 show measured transients in current density at a constant applied potentials of 900 and 1100 mV verses OCP for several different materials in natural seawater at 90°C. The materials compared in each figure include wrought Alloy C-22 (reference material), a fully dense and completely amorphous melt-spun ribbon (MSR) of SAM2X5, HVOF coatings produced with −53/+30 micron powders of SAM2X5, and HVOF coatings produced with −30/+15 micron powders of SAM2X5. The constant potential was applied after 1 hour at the open circuit corrosion potential (OCP). The passive film on the melt spun ribbon and HVOF coatings of SAM2X5 is more stable than that on wrought nickel-based Alloy C-22 under these conditions, leading to the conclusion that this iron-based amorphous metal has superior corrosion resistance.

Transients in current density at a constant applied potential of 900 mV verses OCP for wrought Alloy C-22 (reference material), a fully dense and completely amorphous MSR of SAM2X5, HVOF coatings produced with −53/+30 micron powders of SAM2X5, and HVOF coatings produced with −30/+15 micron powders of SAM2X5, all in natural seawater heated to 90°C, are compared in Figure 10. The constant potential was applied after 1 hour at the open circuit corrosion potential (OCP). It should also be noted that the periodic current fluctuations observed during testing of Alloy C-22 are real, and are indicative of the onset of localized

corrosion. The HVOF coating prepared with relatively fine (−30/+15 μm) SAM2X5 powder has a temporary loss of passivity at 5×10^4 seconds, but undergoes repassivation at 5×10^4 seconds. In contrast, the coating produced with the standard HVOF cut of powder (−53/+30 μm) appears to be completely stable, as does the melt-spun ribbon. The differences in the corrosion resistance of the SAM2X5 coatings produced with relatively coarse (−53/+30 μm) and relatively fine (−30/+15 μm) powders is not well understood, but may be related to differences in surface area. The passive film on the melt spun ribbon and HVOF coatings of SAM2X5 is more stable than that on wrought nickel-based Alloy C-22 under these conditions, leading to the conclusion that this iron-based amorphous metal has superior corrosion resistance.

Transients in current density at a constant applied potential of 1100 mV verses OCP for wrought Alloy C-22 (reference material), a fully dense and completely amorphous MSR of SAM2X5, HVOF coatings produced with −53/+30 micron powders of SAM2X5, and HVOF coatings produced with −30/+15 micron powders of SAM2X5, all in natural seawater heated to 90°C, are compared in Figure 11. The constant potential was applied after 1 hour at the open circuit corrosion potential (OCP). In this case, the passivity of Alloy C-22 was completely lost, with a dramatic increase in the observed current density to levels between 80 and 90 $\mu A/cm^2$, with dramatic attack of the Alloy C-22. A significant difference was observed between the corrosion resistance of HVOF SAM2X5 coatings produced with coarse (−53/+30 μm) and fine (−30/+15 μm) powders, with the standard coarse powder having better performance. The coating produced with the finer powder (−30/+15 μm) did not exhibit good passivity, defined as a current density less than approximately 5 $\mu A/cm^2$, until 2×10^4 seconds, with fluctuations in current density that may be indicative of localized corrosion phenomena. Passivity appears to have been compromised at 7×10^4 seconds. The coating produced with the coarse (−53/+30 μm) powder and the melt-spun ribbon both maintained exceptional passivity during the entire test. In summary, the passive film on the melt spun ribbon and HVOF coatings of SAM2X5 is more stable than that on wrought nickel-based Alloy C-22 under these conditions, leading to the conclusion that this iron-based amorphous metal has superior corrosion resistance.

Standard Test Solutions Used for Immersion Testing

In addition of natural seawater and 3.5-molal sodium chloride solutions, several standardized test solutions have been developed based upon the well J-13 water composition determined by Harrar et al. [29]. Relevant test environments are assumed to include simulated dilute water (SDW), simulated concentrated water (SCW), and simulated acidic water (SAW) at 30, 60, and 90°C. The compositions of all of the test solutions derived from well J-13 water are given in Table 2. The compositions of these test media are based upon the work of Gdowski et al. [30-33]. In general, anions such as chloride promote localized corrosion, whereas other anions such as nitrate tend to act as corrosion inhibitors. Thus, there is a very complex synergism of corrosion effects in the test media.
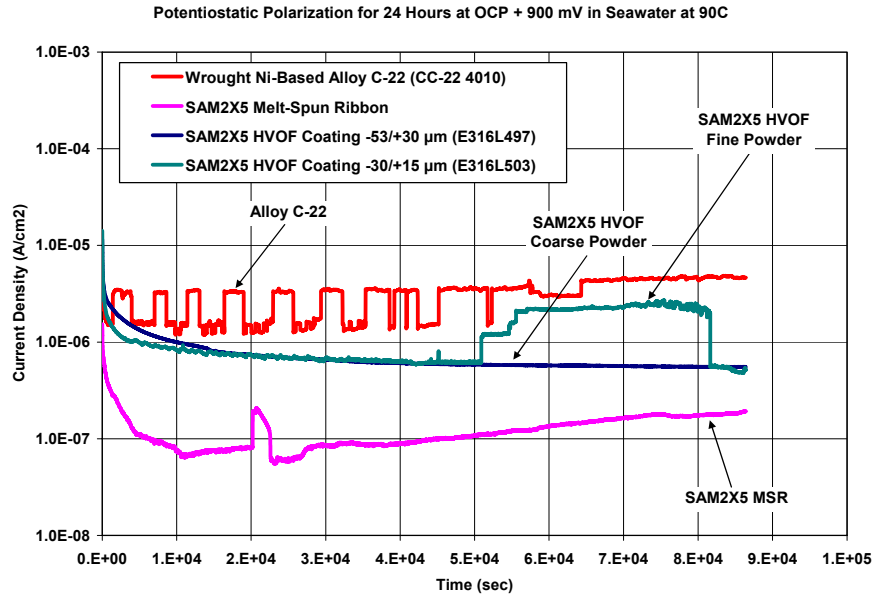
Figure 10 – Transients in current density at a constant applied potential of 900 mV verses OCP for wrought Alloy C-22 (reference material), a fully dense and completely amorphous melt spun ribbon (MSR) of SAM2X5, HVOF coatings produced with –53/+30 micron powders of SAM2X5, and HVOF coatings produced with –30/+15 micron powders of SAM2X5, all in natural seawater heated to 90℃, are compared [Farmer et al. 2006].
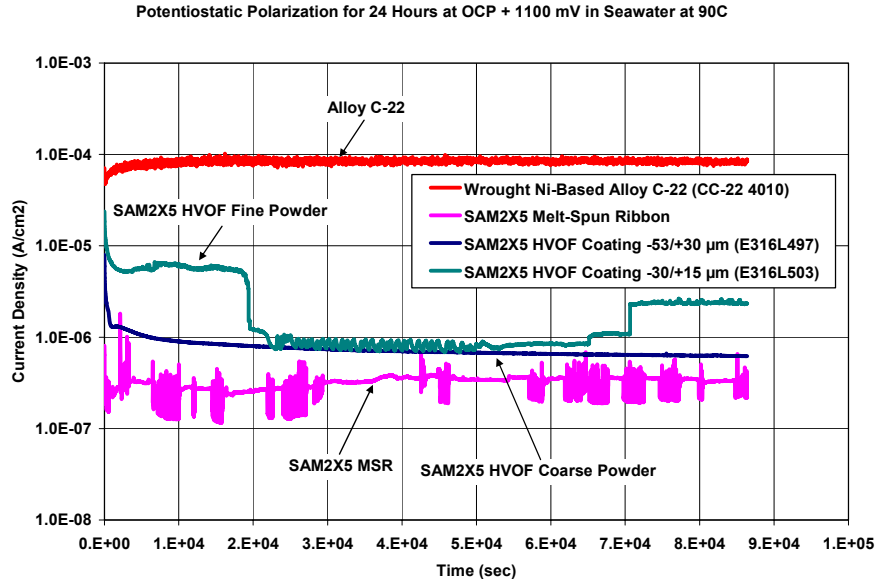

Figure 11 – Transients in current density at a constant applied potential of 1100 mV verses OCP for wrought Alloy C-22 (reference material), a fully dense and completely amorphous melt spun ribbon (MSR) of SAM2X5, HVOF coatings produced with –53/+30 micron powders of SAM2X5, and HVOF coatings produced with –30/+15 micron powders of SAM2X5, all in natural seawater heated to 90℃, are compared [Farmer et al. 2006].

14

Table 2 – Standard test solutions based upon well J-13 water [Gdowski et al. 1997]

Ion	SDW	SCW	SAW
	(mg/L^{-1})	(mg/L^{-1})	(mg/L^{-1})
K^{+1}	34	3,400	3,400
Na^{+1}	409	40,900	40,900
Mg^{+2}	1	1	1,000
Ca^{+2}	1	1	1,000
F^{-1}	14	1,400	0
Cl^{-1}	67	6,700	6,700
NO$_3$$^{-1}$	64	6,400	6,400
SO$_4$$^{-2}$	167	16,700	16,700
HCO$_3$$^{-1}$	947	70,000	0
Si (60°C)	27	27	27
Si (90°C)	49	49	49
pH	8.1	8.1	2.7

Corrosion Rate Determination During Immersion Testing

The linear polarization method was used as a method for determining the corrosion rates of the various amorphous metal coatings. The procedure used for linear polarization testing consisted of the following steps: (1) holding the sample for ten seconds at the OCP; (2) beginning at a potential 20 mV below the OCP, increasing the potential linearly at a constant rate of 0.1667 mV per second to a potential 20 mV above the OCP; (3) recording the current being passed from the counter electrode to the working electrode as a function of potential relative to a standard Ag/AgCl reference electrode; and (4) determining the parameters in the cathodic Tafel line by performing linear regression on the voltage-current data, from 10 mV below the OCP, to 10 mV above the OCP. The slope of this line was the polarization resistance, *Rp* (ohms), and was defined in the published literature [33].

$$R_P = \left(\frac{\partial E}{\partial I} \right)_{E_{corr}} \tag{3}$$

A parameter (*B*) was defined in terms of the anodic and cathodic slopes of the Tafel lines:

$$B = \frac{\beta_a \beta_c}{2.303(\beta_a + \beta_c)} \tag{4}$$

Values of B were published for a variety of iron-based alloys, and varied slightly from one alloy-environment combination to another [33]. Values for carbon steel, as well as Type 304, 304L and 430 stainless steels, in a variety of electrolytes which include seawater, sodium chloride, and sulfuric acid, ranged from 19 to 25 mV. A value for nickel-based Alloy 600 in lithiated water at 288°C was given as approximately 24 mV. While no values have yet been developed for the Fe-based amorphous metals that are the subject of this investigation, it was believed that a conservative representative value of approximately 25 mV was appropriate for the conversion of

polarization resistance to corrosion current. Given the value for Alloy 600, a value of 25 mV was also believed to be acceptable for converting the polarization resistance for nickel-based Alloy C-22 to corrosion current. The corrosion current density, i_{corr} (A cm^{-2}), was defined in terms of the Tafel parameter (B), the polarization resistance (Rp), and the actual electrode area (A):

$$i_{corr} = \frac{B}{R_p \times A}$$
(5)

The corrosion (or penetration) rates of the amorphous alloy and reference materials were calculated from the corrosion current densities with the following formula:

$$\frac{dp}{dt} = \frac{i_{corr}}{\rho_{alloy} n_{alloy} F}$$
(6)

where p was the penetration depth, t was time, i_{corr} was the corrosion current density, ρ_{alloy} was the density of the alloy (g cm^{-3}), n_{alloy} was the number of gram equivalents per gram of alloy, and F was Faraday's constant. The value of n_{alloy} was calculated with the following formula:

$$n_{alloy} = \sum_j \left(\frac{f_j n_j}{a_j} \right)$$
(7)

where f_j was the mass fraction of the jth alloying element in the material, n_j was the number of electrons involved in the anodic dissolution process, which was assumed to be congruent, and a_j was the atomic weight of the jth alloying element. Congruent dissolution was assumed, which meant that the dissolution rate of a given alloy element was proportional to its concentration in the bulk alloy. These equations were used to calculate factors for the conversion of corrosion current density to the penetration rate (corrosion rate).

Corrosion rates and open-circuit corrosion potentials of HVOF SAM2X5 and SAM1651 coatings were determined in situ during long-term immersion testing in several relevant environments and are reported here. Since these as-sprayed samples were very rough, an estimated roughness factor of 3.36 was used to convert apparent surface area to actual surface area. Figures 12 and 13 show OCP values and corrosion rates for amorphous SAM2X5 (Lot #06-015) and SAM1651 coatings in seawater, 3.5-molal NaCl solutions, and synthetic bicarbonate brines (SDW, SCW and SAW). Based upon the corrosion rates of SAM2X5 coatings, solutions are ranked from least- to most-aggressive: SDW at 90°C; 3.5-molal NaCl with 0.525-molal KNO$_3$ solution at 90°C; seawater at 90°C; 3.5-molal NaCl solution at 30°C; SCW at 90°C; SAW at 90°C; and 3.5-molal NaCl solution at 90°C. The ranking for SAM1651 coatings is slightly different. Examples of the corrosive attack of both SAM2X5 and SAM1651 HVOF coatings after long-term immersion in seawater, 3.5 m NaCl with 0.625 m KNO3, SDW and SAW, all at 90°C, are shown in Figure 14. The samples shown in this figure are the coated rods used for long-term OCP and linear polarization measurements.

Based upon corrosion rate data, as well at visual differences, it is concluded that SAM1651 may perform slightly better than SAM2X5 in some environments, such as seawater at 90°C (Figures 14a and 14b). The SAM1651 showed the formation of slight superficial red iron oxide in some solutions at elevated temperature (Figure 14h).
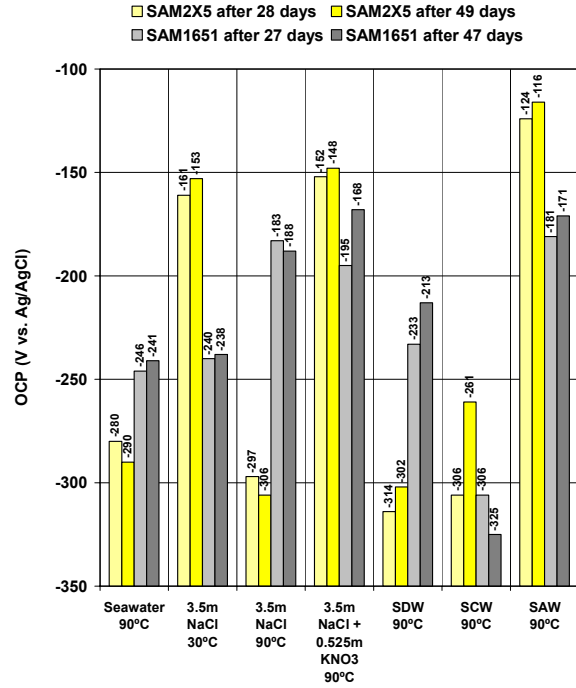
Figure 12 – Comparison of open-circuit potential (OCP) values for as-sprayed SAM2X5 and SAM1651 coatings [Farmer et al. 2007].
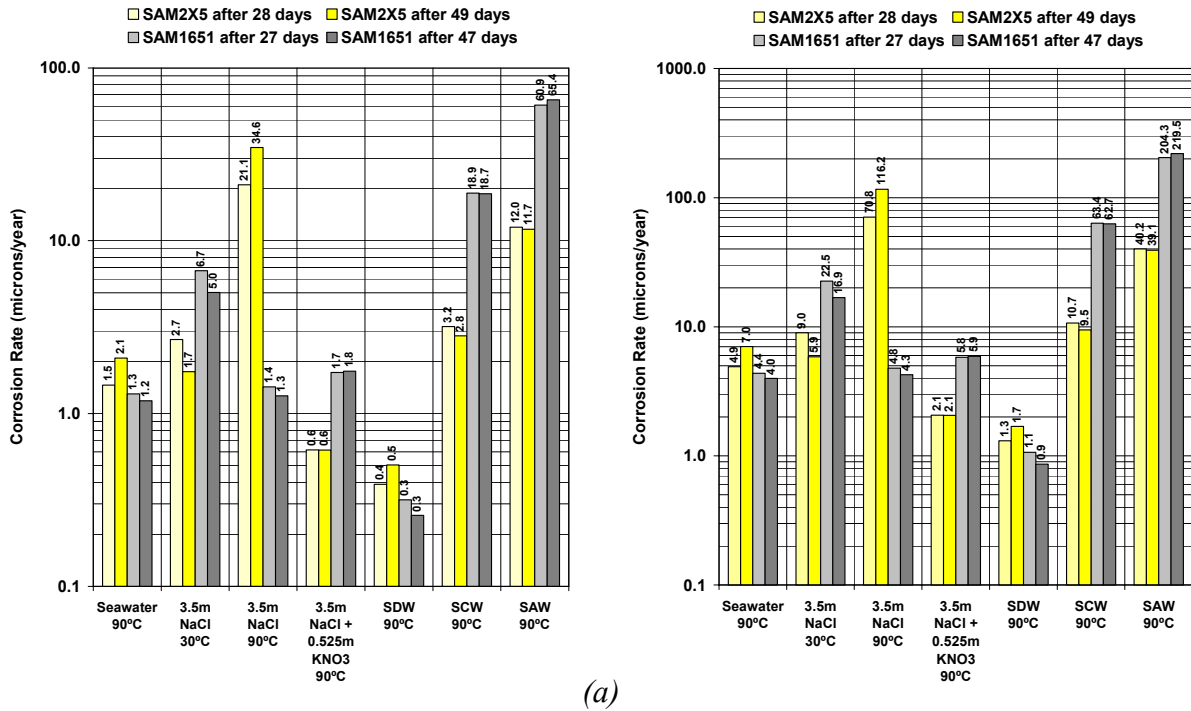

Figure 13 – Corrosion rate values for as-sprayed SAM2X5 and SAM1651 coatings determined with linear polarization: (a) estimated roughness factor of approximately 3.36 assumed to account for the as-sprayed surface; and (b) no roughness factor assumed [Farmer et al 2007].
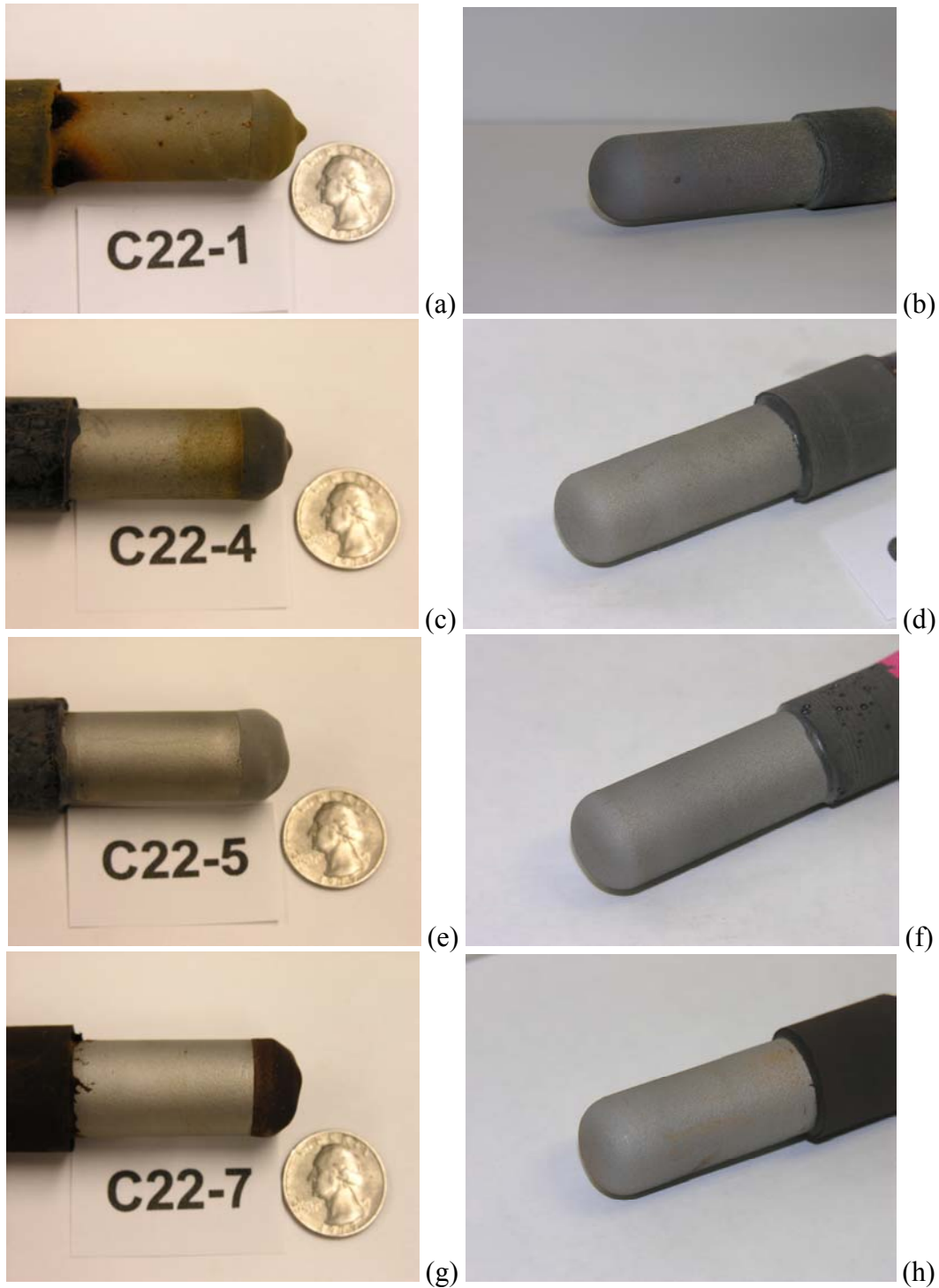
17

Figure 14 – Examples of corrosive attack after long-term immersion exposure of: (a) SAM2X5 and (b) SAM1651 to natural seawater 90°C; (c) SAM2X5 and (d) SAM1651 to 3.5m NaCl + 0.625m KNO₃ at 90°C; (e) SAM2X5 and (f) SAM1651 to SDW at 90°C; and (g) SAM2X5 and (h) SAM1651 to SAW at 90°C. Long-term immersions were 134 and 112 days for SAM2X5 and SAM1651, respectively.

Corrosion of these coatings appears to be superficial, with no detectable corrosion penetrating to the substrate. This is illustrated with the scanning electron micrographs and elemental maps of a coating on a planar substrate, after immersion in seawater at 90C for 112 days. Images of the cross-section are shown in Figures 15 and 16.
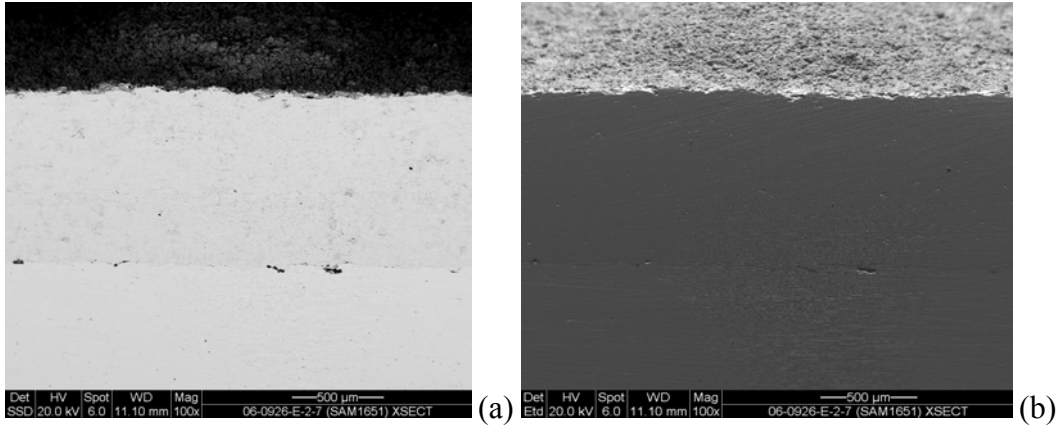

Figure 15 – Metallographic cross-sections of slightly corroded region of SAM1651 (V5793) coated on C22 after approximately 112 days (16 weeks) at open circuit in 90°C seawater: (a) back-scattered electron image; (b) secondary electron image.
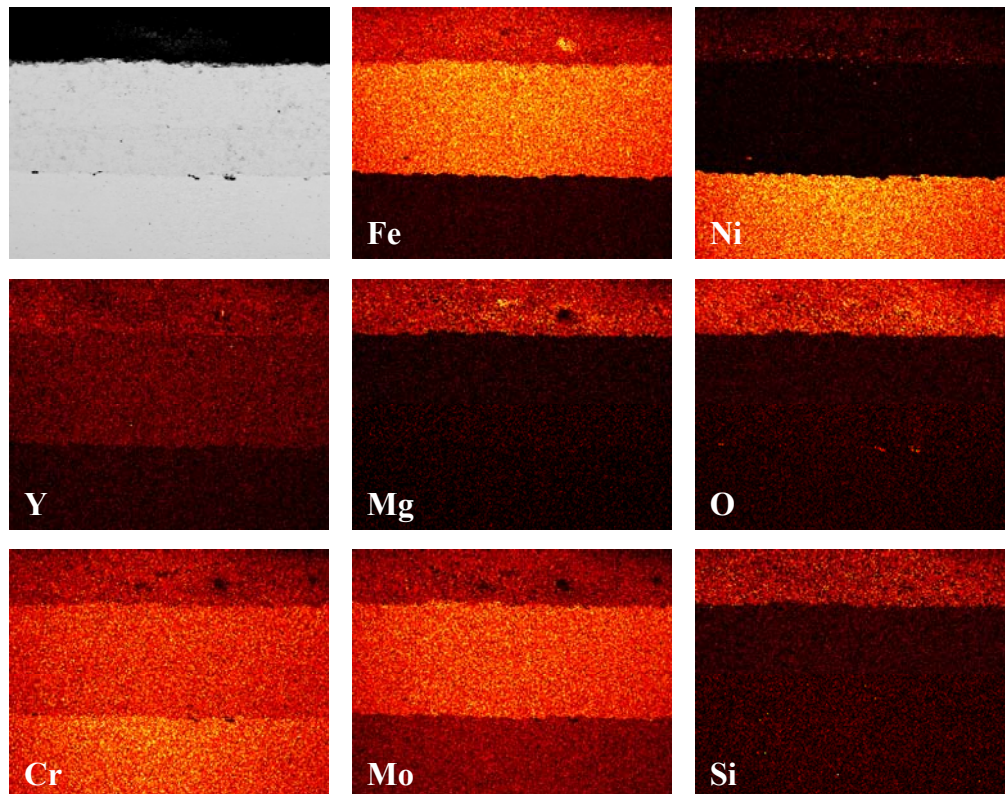

Figure 16 – Metallographic cross-sections of slightly corroded region of SAM1651 (V5793) coated on C22 after approximately 112 days (16 weeks) at open circuit in 90°C seawater: elemental mapping of Fe, Ni, Y, Mg, O, Cr, Mo and Si with energy dispersive spectroscopy (EDS).

Formulations Exist with Potentially Better Corrosion Resistance

Other amorphous alloys may be more corrosion resistant than the SAM1651 and SAM2X5 discussed here. In addition to synthesizing these alloys, melt-spun ribbon (MSR) samples of $Fe_{43}Cr_{16}Mo_{16}B_5C_{10}P_{10}$ (SAM6) were also prepared [6]. As shown in Figure 16, while MSR samples of Alloy 22 were completed dissolved in hydrochloric acid after several-days exposure (left), MSR samples with SAM6 composition did not dissolve (right).
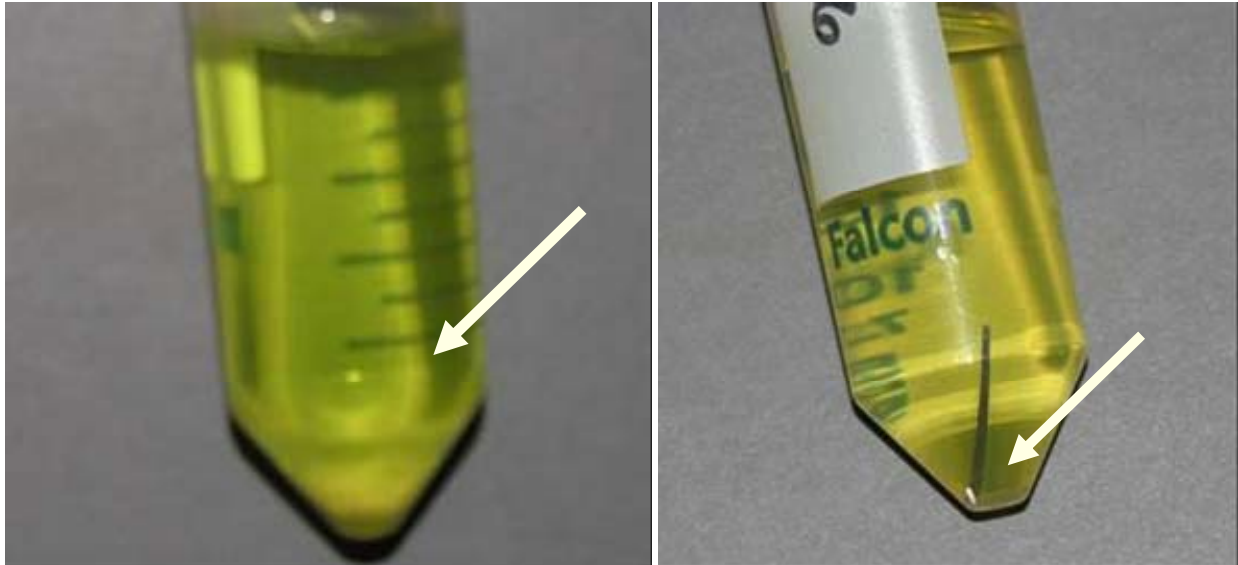

Figure 17 – Alloy C-22 dissolved in concentrated HCl (left), while a melt-spun ribbon of SAM6 remained intact for an exposure lasting several months (right). Extreme corrosion resistance is possible with iron-based amorphous metals [Farmer et al. 2007].

Salt Fog Testing

Salt fog tests were conducted according to the standard General Motors (GM) salt fog test, identified as GM9540P. The protocol for this test is summarized in Table 4. The salt solution mists (denoted with asterisks) consisted of 1.25% solution containing 0.9% sodium chloride, 0.1% calcium chloride, and 0.25% sodium bicarbonate. The four reference samples included Type 316L stainless steel, nickel-based Alloy C-22, Ti Grade 7, and the 50:50 nickel-chromium binary.

Salt fog tests were conducted according to the standard General Motors (GM) salt fog test, identified as GM9540P, or an abbreviation of that test [34]. Thermal-spray coatings of SAM2X5 and SAM1651 coatings were tested, with 1018 steel serving as control samples. After eight cycles in this salt-fog test, SAM2X5 and SAM1651 coatings on flat plates and a half-scale spent nuclear fuel (SNF) prototypical container proved to be corrosion resistant, whereas the steel reference samples underwent aggressive attack.

Table 3 – A description of the standard GM9540P Salt Fog Test is summarized here. Note that the salt solution mistsconsisted of 1.25% solution containing 0.9% sodium chloride, 0.1% calcium chloride, and 0.25% sodium bicarbonate [Aprigliano et al. 2006]

24-Hour Test Cycle for GM9540P Accelerated Corrosion Test		
Shift	Elapsed Time (hrs)	Event
Ambient Soak	0	Salt solution mist for 30 seconds, followed by ambient exposure at 13-28°C (55-82°F)
	1.5	Salt solution mist for 30 seconds, followed by ambient exposure at 13-28°C (55-82°F)
	3	Salt solution mist for 30 seconds, followed by ambient exposure at 13-28°C (55-82°F)
	4.5	Salt solution mist for 30 seconds, followed by ambient exposure at 13-28°C (55-82°F)
Wet Soak	8 to 16	High humidity exposure for 8 hours at 49 ± 0.5°C (120 ± 1°F) and 100% RH, including a 55-minute ramp to wet conditions
Dry Soak	16 to 24	Elevated dry exposure for 8 hours at 60 ± 0.5°C (140 ± 1°F) and less than 30% RH, including a 175-minute ramp to dry conditions

Photographs of samples after eight full cycles in the GM salt-fog test described in Table 4 are shown in Figure 17. These samples are: (a) 1018 carbon steel reference specimens [Samples # A14]; (b) HVOF coating of SAM2X5 on Type 316L stainless steel substrate [Sample # 316L-W9], HVOF coating of SAM2X5 on nickel-based Alloy C-22 substrate [Sample # C22-W21], and HVOF coating of SAM2X5 on half-scale spent nuclear fuel (SNF) container made of Type 316L stainless steel, all after 8 full cycles in GM salt fog test. Clearly, the thermal-spray coatings of SAM2X5 have good resistance to corrosive attack in such environments. Similar testing wad done with a half-scale SNF container coated with SAM1651. This SAM1651-coated cylinder, after salt fog testing, is shown in Figure 18. Some running rust was observed on one bottom of the container, which may be due to surface preparation prior to coating.
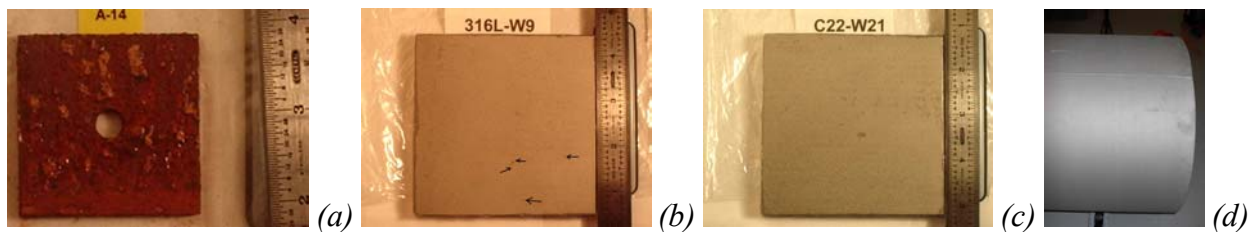

(a) *(b)* *(c)* *(d)*

Figure 18 – Photographs of three samples after eight full cycles in the GM salt-fog test: (a) 1018 carbon steel reference sample; (b) SAM2X5 Lot # 06-015 on 316L plate; (c) SAM2X5 Lot # 06-015 on Alloy C-22 plate; and (d) SAM2X5 Lot #0-6-015 on 316L half-scale SNF container.
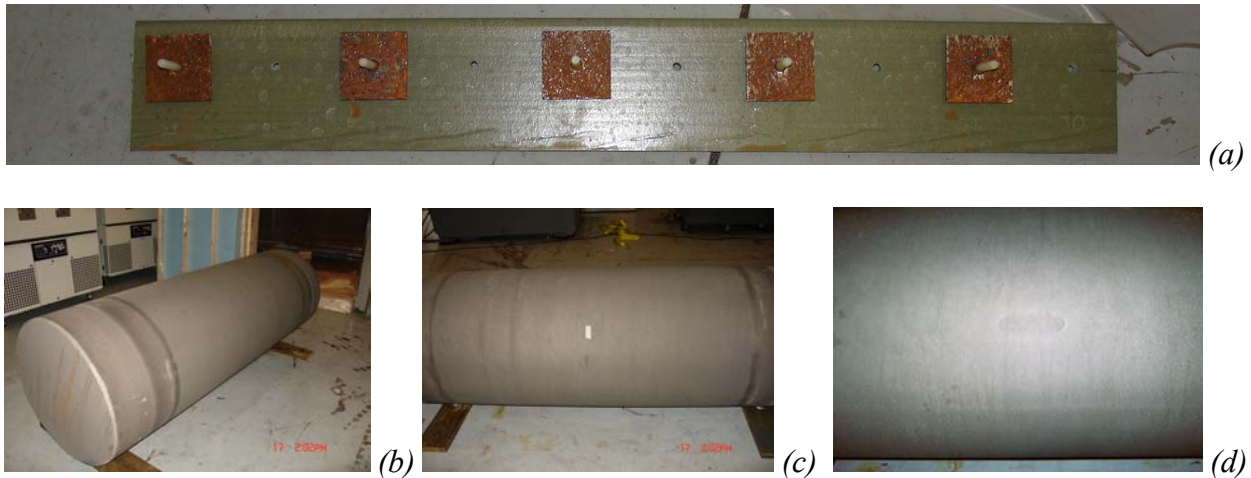
Figure 19 – Effect of GM9540P salt-fog test on: (a) 1018 steel reference samples; (b-d) HVOF coating of SAM1651 amorphous metal on half-scale SNF prototypical container (bottom)

Damage Tolerance

Figure 19a shows the non-destructive ultrasonic measurement of plate M17S1 before impact testing. The corner in the upper right was intentionally surface ground down to the level of the Alloy 22 substrate to reveal the amount of energy reflected by a completely unbonded coating. This particular plate appeared to have more variability as observed by the slight color difference at the bottom right and upper right. Note that the edges (~1/4") of the plate should be ignored since a focused transducer was used which is affected by edges of the substrate. Also the signal results in this figure have been mirrored appropriately so that the positions of the impacts can be identified in the associated optical photograph. This is required because the ultrasound measurements are taken from the back of the plate.

Figures 19b and 19c show plate M17S3 after impact testing with the range of conditions given in Table 5. The slight yellow lines reflect cracks observed in some cases on the surface. The large areas with colors above red and yellow on the scale are regions where greater reflected energy is observed at the interface. A transition to greater reflected energy at the interface for the impacts on the left hand side of the plate is observed. The larger regions of higher reflected energy around the impacts appears to be consistent with the before impact Ultrasonic NDE measurements. Note that the edges (~1/4") of the plate should be ignored since a focused transducer was used which is affected by edges of the substrate. Also the signal results in this figure have been mirrored appropriately so that the positions of the impacts can be identified in the associated optical photograph. This is required because the ultrasound measurements are taken from the back of the plate.

Table 4 – Impact velocities used during drop-tower testing of Alloy C-22 plates coated with SAM2X5 powder (Lot # 05-079) [Haslam et al. 2006]

Impact #	Insert Diameter	Impact Velocity	Drop Weight	Max. Load	Total energy
	(in)	**(ft sec⁻¹)**	**(lb)**	**(lb)**	**(ft lbf)**
1	0.5	9.97	16.35	8,563	23.37
2	0.5	9.98	16.35	8,500	23.28
3	0.5	9.95	16.35	9,462	22.63
4	0.5	19.13	16.19	20,146	76.11
5	0.5	19.16	16.19	20,220	76.61
6	0.5	19.29	16.19	20,567	78.22
7	0.5	29.73	16.19	31,688	183.55
8	0.5	29.65	16.19	30,720	183.13
9	0.5	29.58	16.19	33,021	182.84
10	0.5	42.57	16.15	*43,000	286.70
11	0.5	43.14	16.25	*42,000	309.91
13	0.5	19.69	27.76	30,306	144.16
14	0.5	19.69	27.76	29,917	145.64
15	1.0	19.11	16.61	19,684	84.51
16	1.0	19.22	16.61	20,638	84.88

Header rows of table:
Impact Testing of Plate M17S3
1-Inch Thick Alloy C-22 Plate Coated with SAM2X5 Lot # 05-079
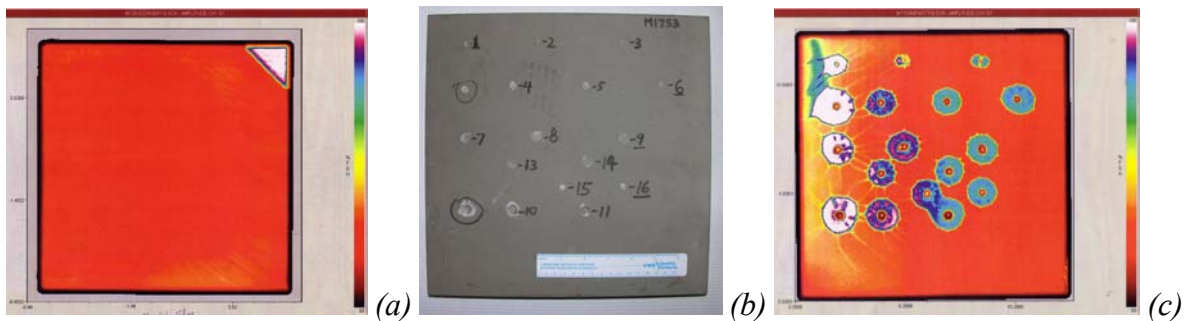

(a) (b) (c)

Figure 20. Images of SAM2X5-coated plates subjected to drop-tower testing at LLNL: (a) ultrasonic non-destructive evaluation prior to impact; (b) photographs showing visible damage of after impact at various impact velocities; (c) ultrasonic non-destructive evaluation showing damage underneath coating at various impact velocities [Haslam et al. 2006].

Neutron Absorption

The high boron content of $Fe_{49.7}Cr_{17.7}Mn_{1.9}Mo_{7.4}W_{1.6}B_{15.2}C_{3.8}Si_{2.4}$ (SAM2X5) makes it an effective neutron absorber, and suitable for criticality control applications. Average measured values of the neutron absorption cross section in transmission (Σ_t) for Type 316L stainless steel, Alloy C-22, borated stainless steel, a Ni-Cr-Mo-Gd alloy, and SAM2X5 have been determined to be approximately 1.1, 1.3, 2.3, 3.8 and 7.1, respectively [22]. Data are sown in Table 6 and Figure 20. This material and its parent alloy have been shown to maintain corrosion resistance up to the glass transition temperature, and to remain in the amorphous state after receiving relatively high neutron dose.
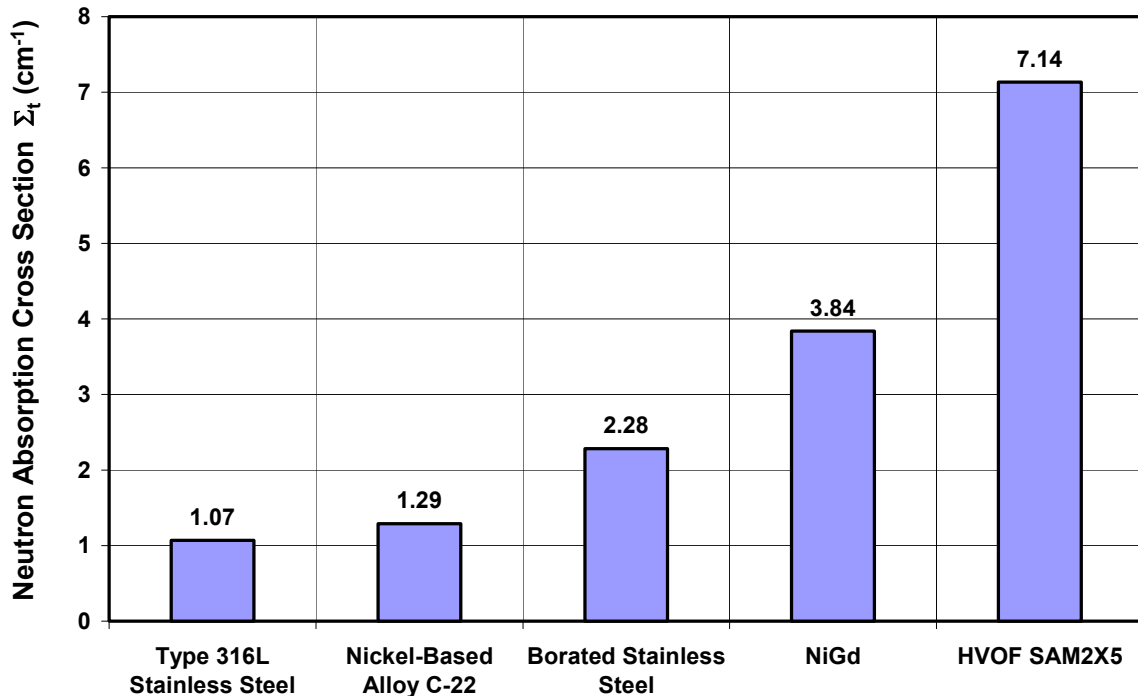

Figure 21 – Average measured values of the neutron absorption cross section in transmission (Σ_t) for Type 316L stainless steel, Alloy C-22, borated stainless steel, a Ni-Cr-Mo-Gd alloy, and SAM2X5.

Materials used in criticality control applications must be relatively stable during irradiation with thermal neutrons. Melt-spun ribbon samples of various iron-based amorphous metals were subjected to high neutron dose in the 1.5 MW TRIGA reactor at McClellan Nuclear Radiation Center (MNRC) [22]. The neutron flux was 1.6×10^{10} n cm^{-2} sec^{-1}. Samples were irradiated for three different times: duration of 1st irradiation was 44 minutes; duration of 2nd irradiation was 132 minutes; and duration of 3rd irradiation was 263 minutes. The corresponding neutron doses were: 4.3×10^{13} n cm^{-2}, 1.3×10^{14} n cm^{-2} sec^{-1} and 2.6×10^{14} n cm^{-2}, respectively. These doses are equivalent to approximately 670, 2000 and 4000 years inside the waste packages designed for emplacement at Yucca Mountain. As shown in Figure 21, an exposure corresponding to a 4000-year service life does not cause any detectable, deleterious phase transformations. The neutron exposure is summarized in Table 7.
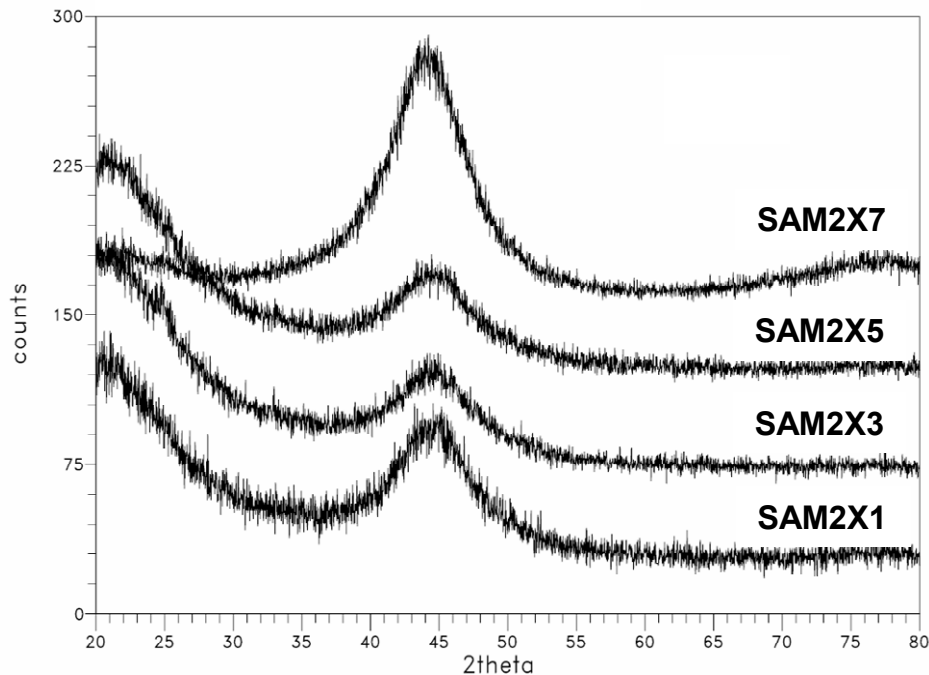
Figure 22 – XRD of high-boron iron-based SAM2X-series of amorphous-metal alloys after 3rd irradiation at MNRC.

Possible Applications

Safe Storage of Spent Nuclear Fuel

SAM2X5 may have beneficial for applications such as the safe long-term storage of spent nuclear fuel [34-36]. These materials have exceptional neutron absorption characteristics, and are stable at high dose. The absorption cross section in transmission for thermal neutrons for SAM2X5 coatings is three to four times (3 to 4×) greater than that of borated stainless steel, and twice (2×) as good as nickel-based Alloy C-4 with additions of Gd (Ni-Cr-Mo-Gd) [22]. It may be possible to achieve substantial cost savings by substituting these new Fe-based materials for more expensive Ni-Cr-Mo and Ni-Cr-Mo-Gd alloys. Thermal spray coatings of Fe-based amorphous metals are predicted to cost ~ $7 per pound, whereas plates of Ni-Cr-Mo are expected to cost ≥ $37 per pound, based upon actual purchase costs of Alloy C-22, without additions of gadolinium.

Simulations and design calculations at LLNL show that k-effective can be lowered by at least ten percent (10 %) with the application of 1-millimeter thick coating of SAM2X5 to SNF support structure (basket) in 21-PWR container [22]. Even better performance is possible through the use of enriched boron for the synthesis of the Fe-based amorphous metal. The Fe-based amorphous metals have already been produced in multi-ton quantities and should cost less than $10 per pound, while relatively few (three-or-four) 300-pound heats have been made of the Ni-Gd Material, which may cost nearly $40 per pound.

Tunnel Boring Applications

The hardness values for Type 316L stainless steel, nickel-based Alloy C-22, and HVOF SAM2X5 are 150, 250 and 1100-1300 VHN, respectively. These materials are extremely hard and provide enhanced resistance to abrasion and gouges. In fact, successful tests have been conducted for applications as disk cutters for the tunnel boring machines.

Deterioration of Nation's Infrastructure

The infrastructure for transportation in the United States allows for a high level of mobility and freight activity for the current population of 300 million residents, and several million business establishments. According to a Department of Transportation study, more than 230 million motor vehicles, ships, airplanes, and railroads cars were used on 6.4 million kilometers (4 million miles) of highways, railroads, airports, and waterways in 1998. Pipelines and storage tanks were considered to be part of this deteriorating infrastructure. The annual direct cost of corrosion in the infrastructure category was estimated to be approximately $22.6 billion in 1998 [37].

There were 583,000 bridges in the United States in 1998. Of this total, 200,000 bridges were steel, 235,000 were conventional reinforced concrete, 108,000 bridges were constructed using pre-stressed concrete, and the balance was made using other materials of construction. Approximately 15 percent of the bridges accounted for at this point in time were structurally deficient, primarily due to corrosion of steel and steel reinforcement. The annual direct cost of corrosion for highway bridges was estimated at $8.3 billion to replace structurally deficient bridges over a 10-year period of time, $2 billion for maintenance and cost of capital for concrete bridge decks, $2 billion for maintenance and cost of capital for concrete substructures, and $0.5 billion for maintenance of painting of steel bridges. Life-cycle analysis estimates indirect costs to the user due to traffic delays and lost productivity at more than 10 times the direct cost of corrosion maintenance, repair and rehabilitation [37].

In the early 1970's on epoxy-coated reinforcing steel (ECR) was qualified as an alternative to black bar to help address the problems associated with corrosion. For the past 30 years, ECR has been specified by several State Departments of Transportation for major decks and sub-structures exposed to chlorides. At the same time, ECR was augmented by use of low water-to-cement ratio (w/c) concrete, possibly with corrosion inhibitors. However, in Florida coastal waters, ECR has proven ineffective because of the combined effects of higher average temperature and more prolonged moist exposure [38].

The Innovative Bridge Research and Construction (IBRC) Program was authorized by Congress in the Transportation Equity Act for the 21st Century legislation initially as a 6-year effort (1998-2003), but was subsequently extended through May 2005. The majority of the funding was for actual repair, rehabilitation and replacement of existing structures, and for new construction with a lesser amount for research, both based upon innovative materials. Corrosion-resistant reinforcements constituted one component of the program. Reinforcement materials included black bar, epoxy-coated reinforcing steel (ECR), solid stainless steel (Types 316LN and 2205), clad stainless steel, galvanized steel and others [38].

Since the IBRC Program, new iron-based amorphous metals with good corrosion resistance have been developed, along with the technology necessary for applying these materials as coatings to large-area substrates, including steel reinforcing bars. It is believed that these coatings may be able to substantially enhance the corrosion resistance steel reinforcements

in concrete structures. This proposal aims to evaluate these new advanced materials as a practical means of enhancing the performance of steel reinforcing bars.

Potential Economic Benefits for Storage of Spent Nuclear Fuel & High-Level Waste

A cost model was developed and used to predict the cost to produce Type 316 stainless steel, nickel-based Alloys C-276 and C-22, and the iron-based amorphous metals discussed here. This assumed cost of the raw materials required to produce all of these materials were taken from compilations of the United States Geological Survey (USGS). Based upon these assumptions, the predicted costs for nickel-based Alloys C-276 and C-22 were $22-23/lb. The most recent procurements of Alloy C-22 by these authors was at a cost of $37/lb. More exotic nickel-based alloys proposed for use as criticality control materials, such at Ni-Cr-Mo-Gd will cost even more due to the incorporation of gadolinium as a neutron poison. The cost of Type 316L stainless steel is estimated to be approximately $7/lb. HVOF coatings of SAM2X5 and SAM1651 are predicted to cost $7 to $10 per pound. It is important to note that these costs are predictions, intended to illustrate the potential savings by substituting iron-based materials for more expensive nickel-based materials, and do not represent actual purchase prices.

The cost savings possible by substituting iron-based amorphous metals for more expensive nickel and titanium alloys in a high-level waste repository were predicted. Assuming acceptable materials performance is demonstrated, the following cost savings may ultimately be possible for fabrication of containers, support pallets, and drip shields, all required for emplacement spent nuclear fuel and high-level radioactive waste at the proposed repository at Yucca Mountain. Additional analyses should be done in the future for the criticality control application.

1. Assume $3/lb: Substantial savings are realized for the waste package (42% ~ $881 million), pallets (24% ~ 41 million), and drip shield (81% ~ $2.8 billion).
2. Assume $6/lb: Reasonable savings (7% ~ 271 million) for the waste package, no savings for the pallet, and large savings for the drip shield (70% ~ $2.5 billion).
3. Assume $8/lb: No savings is achieved for the waste package or pallet, but substantial savings can still be realized for the drip shield (63% ~ $2.3 billion).

The assumptions involved in these predictions are summarized in more detail as follows:

1. Feed Cost = $3/lb (Low); $ 6/lb (Mid Range); $8/lb (High)
2. Throughput = 1 waste package, 1 pallet, 1 drip shield per day
3. Floor Space = 75,000 square feet at $500 per square foot
4. Personnel = 15 FTE at $250,000 per person per year
5. Equipment = 39 HVOF guns (30 lb/hr) at $250,000 per gun
6. Cost of Nickel-Based Wrought Alloy Increasing Rapidly

Conclusions

Early Fe-based amorphous metal coatings had very poor corrosion resistance and failed salt-fog tests. New Fe-based amorphous-metal alloys and thermal-spray coatings based upon these alloys have been developed with good corrosion resistance, high hardness, and exceptional neutron absorption cross sections. More than forty high-performance Fe-based amorphous alloys were systematically designed and synthesized. Cr, Mo and W were added to enhance corrosion resistance; Y was added to lower the critical cooling rate; and B was added to render the alloy amorphous and to enhance capture thermal neutrons. Enriched boron could be used for enhanced

absorption of thermal neutrons. Phase stability has been demonstrated well above 500-600°C and at high neutron dose (equivalent to 4000 years inside Yucca Mountain container). With additional development, it may be possible to use these materials to achieve cost benefits for the fabrication of next-generation spent nuclear fuel containers, and basket assemblies with enhanced criticality safety. Multi-ton quantities of gas-atomized SAM2X5 and SAM1651 powder have been produced and applied as protective coatings on numerous prototypes and parts. These new materials are now under evaluation for several applications of national importance, ranging from defense to infrastructure.

Acknowledgments

References

[1]   M. Telford, The Case for Bulk Metallic Glass. *Materials Today*, Vol. 3, 2004, pp. 36-43

[2]   N. Sorensen and R. Diegle, Corrosion of Amorphous Metals, *Corrosion, Metals Handbook*, 9th Ed., Vol. 13, edited by J. R. Davis and J. D. Destefani, ASME, 1987, pp. 864-870

[3]   D. Polk and B. Giessen, Overview of Principles and Applications, Chapter 1, *Metallic Glasses*, edited by J. Gilman and H. Leamy, ASME, 1978, pp. 2-35

[4]   K. Kishitake, H. Era, and F. Otsubo, Characterization of Plasma Sprayed Fe-10Cr-10Mo-(C,B) Amorphous Coatings, *J. Thermal Spray Tech.*, Vol. 5 (No. 2), 1996, pp. 145-153

[5]   S. Pang, T. Zhang, K. Asami, and A. Inoue, Effects of Chromium on the Glass Formation and Corrosion Behavior of Bulk Glassy Fe-Cr-Mo-C-B Alloys, *Materials Transactions*, Vol. 43 (No. 8), 2002, pp. 2137-2142

[6]   S. Pang, T. Zhang, K. Asami, and A. Inoue, Synthesis of Fe-Cr-Mo-C-B-P Bulk Metallic Glasses with High Corrosion Resistance, *Acta Materialia*, Vol. 50, 2002, pp. 489-497

[7]   F. Guo, S. Poon, and G. Shiflet, Metallic Glass Ingots Based on Yttrium, *Metallic Applied Physics Letters*, Vol. 83 (No. 13), 2003, pp. 2575-2577

[8] Z. Lu, C. Liu, and W. Porter, Role of Yttrium in Glass Formation of Fe-Based Bulk Metallic Glasses, *Metallic Applied Physics Letters*, Vol. 83 (No. 13), 2003, pp. 2581-2583

[9] V. Ponnambalam, S. Poon, and G. Shiflet, *JMR*, Vol. 19 (No. 5), 2004, pp. 1320

[10] D. Chidambaram, C. Clayton, and M. Dorfman, Evaluation of the Electrochemical Behavior of HVOF-Sprayed Alloy Coatings, *Surface and Coatings Technology*, Vol. 176, 2004, pp. 307-317

[11] H. Hack, Crevice Corrosion Behavior of Molybdenum-Containing Stainless Steel in Seawater, *Materials Performance*, Vol. 22 (No. 6), 1983, pp. 24–30

[12] A. Asphahani, Corrosion Resistance of High Performance Alloys, *Materials Performance*, Vol. 19 (No. 12), 1980, pp. 33–43

[13] R. Rebak and P. Crook, Improved Pitting and Crevice Corrosion Resistance of Nickel and Cobalt Based Alloys, *Symposium on Critical Factors in Localized Corrosion III, 194th ECS Meeting*, Vol. 98-17, 1999, pp. 289-302.

[14] Z. Szklarska-Smialowska, Pitting Resistance Equivalence Number, Effect of Alloying Elements on Stainless Steels and Ni-Base Alloys, Chapter 13, *Pitting and Crevice Corrosion*, NACE, 2005, p. 318-321.

[15] A. Sedriks, Introduction, Pitting, Chapter 4, *Corrosion of Stainless Steels*, J. Wiley & Sons, New York, NY, 1996, p. 111-113

[16] D. Agarwal and M. Kohler, Alloy 33, A New Material Resisting Marine Environment, Paper 424, *Corrosion 97*, NACE, 1997

[17] D. Branagan, Method of Modifying Iron-Based Glasses to Increase Crystallization Temperature Without Changing Melting Temperature, U.S. Pat. Appl. No. 20040250929, Filed Dec. 16, 2004

[18] D. Branagan, Properties of Amorphous/Partially Crystalline Coatings. U.S. Pat. Appl. No. 20040253381, Filed Dec. 16, 2004

[19] J. Farmer, J. Haslam, S. Day, T. Lian, C. Saw, P. Hailey, J. Choi, R. Rebak, N. Yang, R. Bayles, L. Aprigliano, J. Payer, J. Perepezko, K. Hildal, E. Lavernia, L. Ajdelsztajn, D. Branagan and M. Beardsely, A High-Performance Corrosion-Resistant Iron-Based Amorphous Metal – The Effects of Composition, Structure and Environment on Corrosion Resistance, *Scientific Basis for Nuclear Waste Management XXX*, Symposium NN, MRS Symposium Series, Vol. 985, 2006

[20] J. Farmer, J. Haslam, S. Day, T. Lian, C. Saw, P. Hailey, J. Choi, N. Yang, C. Blue, W. Peter, J. Payer and D. Branagan, Corrosion Resistances of Iron-Based Amorphous Metals

with Yttrium and Tungsten Additions in Hot Calcium Chloride Brine and Natural Seawater, $Fe_{48}Mo_{14}Cr_{15}Y_2C_{15}B_6$ and W-containing Variants, *Critical Factors in Localized Corrosion 5, A Symposiun in Honor of Hugh Issacs, 210th ECS Meeting*, edited by N. Missert, ECS Transactions, Vol. 3, ECS, 2006

[21] T. Lian, D. Day, P. Hailey, J. Choi and J. Farmer, Comparative Study on the Corrosion Resistance of Fe-Based Amorphous Metal, Borated Stainless Steel and Ni-Cr-Mo-Gd Alloy, *Scientific Basis for Nuclear Waste Management XXX*, Symposium NN, MRS Series, Vol. 985, 2006

[22] J. Choi, C. Lee, J. Farmer, D. Day, M. Wall, C. Saw, M. Boussoufi, B. Liu, H. Egbert, D. Branagan, and A. D'Amato, Application of Neutron-Absorbing Structural Amorphous Metal Coatings for Spent Nuclear Fuel Container to Enhance Criticality Safety Controls, *Scientific Basis for Nuclear Waste Management XXX*, Symposium NN, MRS Symposium Series, Vol. 985, 2006

[23] C. Saw, *X-ray Scattering Techniques for Characterization Tools in the Life Sciences, Nanotechnologies for the Life Science*, edited by Challa Kumar, Wiley-VCH Verlag GmbH and Company, KGaA, Weinheim, 2006

[24] C. Saw and R. B. Schwarz, Chemical Short-Range Order in Dense Random-Packed Models, *J. Less-Common Metals*, Vol. 140, 1988, pp. 385-393

[25] J. Farmer, S. Lu, D. McCright, G. Gdowski, F. Wang, T. Summers, P. Bedrossian, J. Horn, T. Lian, J. Estill, A. Lingenfelter, W. Halsey, General and Localized Corrosion of High-Level Waste Container in Yucca Mountain, Transportation, Storage, and Disposal of Radioactive Materials, ASME, PVP Vol. 408, 2000, pp. 53-70

[26] K. Gruss, G. Cragnolino, D. Dunn, and N. Sridar, Repassivation Potential for Localized Corrosion of Alloys 625 and C22 in Simulated Repository Environments, Paper 149, Corrosion 98, NACE, Houston, TX, 1998

[27] Standard Reference Test Method for Making Potentiostatic and Potentiodynamic Anodic Polarization Measurements, Designation G 5-94, *1997 Annual Book ASTM Standards,* Section 3, Vol. 3.02, pp. 54–57

[28] J. C. Farmer, J. J. Haslam, S. D. Day, T. Lian, C. K. Saw, P. D. Hailey, J. S. Choi, R. B. Rebak, N. Yang, J. H. Payer, J. H. Perepezko, K. Hildal, E. J. Lavernia, L. Ajdelsztajn, D. J. Branagan and L. F. Aprigliano, Corrosion Resistance of Thermally Sprayed High-Boron Iron-Based Amorphous-Metal Coatings – $Fe_{49.7}Cr_{17.7}Mn_{1.9}Mo_{7.4}W_{1.6}B_{15.2}C_{3.8}Si_{2.4}$, J. Matls. Res., Vol. 22, No. 8, 2007, pp. 2297-2311

[29] J. E. Harrar, J. F. Carley, W. F. Isherwood, and E. Raber, Report of the Committee to Review the Use of J-13 Well Water in Nevada Nuclear Waste Storage Investigations, UCID-21867, LLNL, Livermore, CA, 1990

[30] G. E. Gdowski, Formulation and Make-up of Simulated Dilute Water (SDW), Low Ionic Content Aqueous Solution, YMP TIP-CM-06, Rev. CN TIP-CM-06-0-2, LLNL, Livermore, CA, 1997

[31] G. E. Gdowski, Formulation and Make-up of Simulated Concentrated Water (SCW), High Ionic Content Aqueous Solution, YMP TIP-CM-07, Rev. CN TIP-CM-07-0-2, LLNL, Livermore, CA, 1997

[32] G. E. Gdowski, Formulation and Make-up of Simulated Acidic Concentrated Water (SAW), High Ionic Content Aqueous Solution, YMP TIP-CM-08, Rev. CN TIP-CM-08-0-2, LLNL, Livermore, CA, 1997

[33] R. Treseder, R. Baboian, and C. Munger, Polarization Resistance Method for Determining Corrosion Rates, *Corrosion Engineer's Reference Book*, 2nd Ed., NACE, 1991, pp. 65-66

[34] J. C. Farmer, J. S. Choi, C. K. Saw, R. H. Rebak, S. D. Day, T. Lian, P. D. Hailey, J. H. Payer, D. J. Branagan, L. F. Aprigliano, Corrosion Resistance of Amorphous $Fe_{49.7}Cr_{17.7}Mn_{1.9}Mo_{7.4}W_{1.6}B_{15.2}C_{3.8}Si_{2.4}$ Coating, A New Criticality Control Material, UCRL-JRNL-229505, LLNL, Livermore, CA; J. Nuclear Technology, ANS, 2007, Accepted for Publication

[35] J. Farmer, J. Haslam, S. Day, T. Lian, R. Rebak, N. Yang, L. Aprigliano, Corrosion Resistance of Iron-Based Amorphous Metal Coatings, PVP2006-ICPVT11-93835, ASME, New York, NY, 2006

[36] J. Farmer, J. Haslam, S. Day, D. Branagan, C. Blue, J. Rivard, L. Aprigliano, N. Yang, J. Perepezko, M. Beardsley, Corrosion Characterization of Iron-Based High-Performance Amorphous-Metal Thermal-Spray Coatings, PVP2005-71664, ASME, New York, NY, 2005

[37] P. Virmani: Corrosion Costs and Preventative Strategies in the United States, Technical Brief: FHWA-RD-01-157 (FHWA, US DOT, March 2002) 17 p

[38] W. H. Hartt, R. G. Powers, D. K. Lysogorski, M. Paredes, Y. P. Virmani: Job Site Evaluation of Corrosion-Resistant Alloys for Use as Reinforcement in Concrete: FHWA-HRT-06-078 (FHWA, US DOT, March 2002), 78 p.